# Revision 2: Solubility and solution mechanisms of chlorine and fluorine in aluminosilicate melts at high pressure and high temperature.

Celia Dalou, Charles Le Losq, Bjorn O. Mysen and George D. Cody

Geophysical Laboratory
Carnegie Institution of Washington DC
5251 Broad Branch Rd, NW
Washington DC

## ABSTRACT

The solubility and solution behavior of F and Cl in peralkaline aluminosilicate compositions in the systems $Na_2O$-$Al_2O_3$-$SiO_2$ and $K_2O$-$Al_2O_3$-$SiO_2$ have been determined for glasses quenched from melts equilibrated at 1400˚C and 1600ºC in the 1.0-2.5 GPa pressure range. With Al/(Al + Si) increasing from 0 to 0.33 in sodium aluminosilicate melts, F solubility (saturation concentration) increases from 3.3 to 7.4 mol%, whereas Cl solubility decreases from 5.7 to 2.5 mol%. There is no difference in F solubility in sodium or potassium aluminosilicate melts. However, the Cl solubility in potassic aluminosilicate melts is 40-60% lower than in sodic melts with the same Al/(Al + Si) and Na or K mole fraction.

Fluorine depolymerizes the silicate melt structure and forms Si-F, Al-F and Na-F complexes, the proportion of which depends on the melt Al/(Al +Si) ratio. Dissolution of Cl

results in a small degree of depolymerization of Al-free silicate melt, whereas Cl has a polymerizing effect in aluminosilicate melts. In both cases, formation of Na-Cl complexes appears to be the driving solution mechanism.

The differences in F and Cl solution mechanisms result in contrasting depolymerizing effects that become more pronounced with increasing degree of magmatic differentiation. Through such modifications of melt structure, F and Cl have significant effects on magma properties such as viscosity, compressibility and element partitioning.

keywords
Fluorine, Chlorine, solubility, solution mechanism, aluminosilicate melt, ionic complexes, magma degassing

## INTRODUCTION

Because of their effects on magma properties, F and Cl are of particular interest for assessing the dynamics of volcanic systems. They can be used as geochemical tracers that allow us to reconstruct the eruptive dynamics of volcanic edifices, as shown for instance by the study of Villemant and Boudon (1998) focused on Mt Pelée (Martinique, French West Indies) or by the study of Balcone-Boissard et al. (2011) focused on the 79 AD eruption of Vesuvius (Italy). Therefore, knowledge of the solubility and bonding of F and Cl in silicate melts and associated effects on melt structure is of prime importance for geochemical and volcanological problems.

Fluorine and chlorine concentration in magmatic liquids (≤ 1wt%) is rather low compared to $H_2O$ in magmas, yet the halogens can play a significant role during magmatic processes. Dissolved F lowers silicate melt viscosity (Dingwell 1987; 1989; Dingwell et al. 1993; Dingwell and Hess 1998; Giordano et al. 2004) and crystallization temperatures (Wyllie and Tuttle 1961; van Groos and Wyllie 1968; Luth 1988a; Filiberto et al. 2012) in a manner resembling $H_2O$. Our understanding of the effect of Cl on melt properties is considerably less comprehensive. A few studies exist on the effect of Cl on melt physical properties (e.g., Dingwell and Hess 1998; Zimova and Webb 2006; Zimova and Webb 2007) and its effect on liquidus temperatures (Filiberto and Treiman 2009). Chlorine dissolved in peralkaline melt can increase viscosity, but it reduces the liquidus temperature.

The type of fluoride complexes formed in melts determines how F affects silicate melt structure. Results from Raman, Infrared and $^{19}F$ Nuclear Magnetic Resonance (NMR) spectroscopy suggest that F could form Si-F bonds when dissolved in $SiO_2$ melts (Dumas et al. 1982; Duncan et al. 1986). However, as the concentration of Al and alkalis or alkaline earth elements increases, F can also form Al-F bonds as well as alkali or alkaline earth fluoride complexes (Mysen and Virgo 1985a,b; Foley et al. 1986; Luth 1988b). Recent data from $^{19}F$ and $^{29}Si$ Magic Angle Spinning (MAS) NMR spectroscopy for Na-aluminosilicate quenched melts (glasses) have suggested that Na-F and Al-F complexing (with variable Al coordination and variable Si/Al ratio in the F-bearing complexes) is more important than complexes with Si-F bonding (Kohn et al. 1991; Schaller et al. 1992; Stebbins and Zeng 2000; Zeng and Stebbins 2000; Stebbins et al. 2000; Mysen et al. 2004).

For Cl-bearing melts, both viscosity measurements (Dingwell and Hess 1998; Zimova and Webb 2006, 2007; Baasner et al. 2013) and structural data from $^{35}Cl$ MAS NMR

spectroscopy (Stebbins and Du 2002; Sandland et al. 2004; Evans et al. 2008) indicate that Cl preferentially bonds with network modifiers (alkalis and/or alkaline earths). Such solution mechanisms imply that Cl causes silicate melt polymerization and, consistently, dissolution of Cl in peralkaline melts increases their viscosity. However, dissolved Cl produces the opposite effect on the viscosity of peraluminous melts, which decreases upon Cl addition (Baasner et al. 2013). This difference suggests that the effect of Cl on melt structure depends on melt composition. Different solution mechanisms of F and Cl are also reflected by different diffusivity of F and Cl in magmatic melts (Alleti et al. 2007, Balcone-Boissard et al. 2009, Böhm and Schmidt 2013). Indeed, F diffuses one order of magnitude faster than chlorine in phonolitic melts (Balcone-Boissard et al. 2009, Böhm and Schmidt 2013), whereas in basaltic melts, F diffusion is half as fast as Cl (Alleti et al. 2007).

Despite the important and different effect of F and Cl on properties of magmatic melts, little or no systematic efforts have been made to compare their solubility and solution mechanisms in silicate and aluminosilicate melts of similar compositions at similar pressure and temperature conditions. We report here results from experiments on F and Cl solubility and solution mechanisms in peralkaline and meta-aluminous quenched melts in F- or Cl-enriched $Na_2O$-$Al_2O_3$-$SiO_2$ and $K_2O$-$Al_2O_3$-$SiO_2$ systems.

## METHODS

### Experimental methods

Two different sets of starting materials were prepared, one on the joins $Na_2O$-$SiO_2$ and $NaAlO_2$-$SiO_2$ and the second on the joins $K_2O$-$SiO_2$ and $KAlO_2$-$SiO_2$. The F and Cl were added to these starting compositions in the experimental sample container.

Compositions of starting materials are shown in Table 1. In Al-free systems, the NS5 and KS5 compositions used for F solubility experiments stand for $Na_2O•5SiO_2$ and $K_2O•5SiO_2$, respectively. The NS3 and KS3 compositions used for Cl solubility experiments stand for $Na_2O•3SiO_2$ and $K_2O•3SiO_2$, respectively. The NS4 composition used for both F and Cl solubility experiments denotes $Na_2O•4SiO_2$. The aluminum-bearing compositions are denoted NS3Ax, KS3Ax, NS4Ax, NS5Ax and KS5Ax, in which x represents the mol percent $Al_2O_3$, which varied from 2.5 to 12.5. The studied melts are peralkaline (i.e., M/Al > 1, with M = Na or K), such that $Al^{3+}$ can be considered as exclusively in 4-fold coordination in fully polymerized $Q^4$ units charged balanced by the alkalis (see, for example, Mysen and Richet, 2005, chapter 4, for review of the concepts of charge-balance of tetrahedrally-coordinated $Al^{3+}$, and Mysen et al., 2003, for experimental data on $Al^{3+}$ distribution among Q-species in peralkaline aluminosilicate melts). In order to isolate the potential effects of Al/(Al + Si) from changes in melt polymerization, the aluminosilicate compositions were synthesized such that the non-bridging oxygen per tetrahedron (NBO/T) ratio of the melts for a given compositional series does not change with increasing Al/(Al + Si) ratio of the bulk melt (Table 1).

Starting materials were prepared from mixtures of high-purity $Na_2CO_3$ or $K_2CO_3$, $SiO_2$ and $Al_2O_3$, decarbonated by slow heating (50ºC/15 minutes), and then melted for 2 hours at ~100ºC above their liquidi (from 900 to 1400ºC; liquidus data from Osborn and Muan 1960). The melts were quenched to glass, crushed and ground under alcohol for 1h. Before grinding, one piece of glass of each composition was kept for major element analysis (Table 1). The

heating step used for decarbonation was repeated before each experiment in order to prevent possible hydration or carbonation of the starting materials by absorption of $CO_2$ and $H_2O$ from the ambient atmosphere. After this drying step, the powdered starting glasses were immediately loaded into Pt capsules with approximately 10 wt% $F_2$ (as 33 wt% $AgF_2$) or 5 wt% $Cl_2$ (as 23 wt% $PdCl_2$). The loaded capsules were welded shut before high-pressure and temperature experiments.

Experiments were conducted at 1.0 to 2.5 GPa and 1400ºC for NS5Ax, KS5Ax and NS4Ax compositions, and at 1600ºC for NS3Ax and KS3Ax compositions. A 90-minute experimental duration was used for all experiments. This duration was chosen based on F and Cl diffusion data in basaltic melts [Alleti et al. (2007), accounting for pressure effects on diffusion, Dingwell et al. (1985)]. Experiments were performed in 3/4 and 1/2 inch-diameter furnace assemblies (Kushiro 1976) in a solid-media, high-pressure apparatus (Boyd and England 1960) at the Geophysical Laboratory (GL). Three 3 mm-diameter capsules (4 mm-length) were loaded in 3/4 inch-diameter furnace assemblies for 1.0, 1.5 and 2.0 GPa experiments; for 2.5 GPa-experiments, a single 3 mm-diameter capsule was loaded in ½ inch-diameter furnace assemblies. From pressure-calibration with the quartz-coesite transition (Bohlen 1984), the uncertainty is ±0.1 GPa. The experimental temperature was controlled to within ± 5ºC of the set point using $Pt/Pt_{90}Rh_{10}$ thermocouples. The samples were quenched by turning off the power to the furnace, which resulted in an initial (down to about 500ºC) average quenching rate of 100ºC/sec.

After each experiment, the capsules were opened to recover the glass. A portion of the sample was retained for analysis by Raman spectroscopy. The remaining glass was mounted

in epoxy resin and polished for analyses by energy dispersive spectroscopy (EDS) on the scanning electron microscope (SEM).

## Analytical methods

Major elements, F, and Cl were analyzed with a JEOL JSM-6500F field emission scanning electron microscope (FE-SEM) equipped with an energy dispersive spectrometer (EDS) operating at 15 kV with a 0.1 nA beam current. A FE-SEM is more suitable than an electron microprobe for these analyses because the energy dispersive spectrometer, in conjunction with the very low beam current of the FE-SEM, is useful for beam sensitive materials requiring low beam current during analysis (Raudsepp 1995). Although wavelength dispersive spectrometer (WDS) analysis has been suggested to be more precise than EDS analysis for various analytical problems, the accuracy of both methods is comparable for polished glasses (Kuisma-Kursula 2000). Because our samples contain numerous bubbles (Fig. 1) and are very rich in Na and K, elements known to migrate under an electron beam, their analysis is challenging. These problems require use of a low beam current and a defocused electron beam to reduce Na and K migration. The shape and size of the beam area had to be adjusted for each analysis in order to avoid bubbles. The beam was defocused to 25 μm to reduce Na migration and to 25 to 50 μm to reduce K migration.

Pyrope (for Si), scapolite (for Na and Cl), ENAL20 (for Al, GL standard), K1597 (for K, NIST standard), topaz (for F) and $MnO_2$ (for Mn) were used as standards to obtain quantitative elemental analysis. Analytical accuracy and precision was evaluated by replicate

158 measurements of orthoclase, diopside and topaz of known compositions. Counting times used
159 were 50 sec per element.

160 To evaluate possible Na, K, F or Cl loss, several analyses were carried out on the same
161 sample spot. There were no significant compositional changes (within one standard deviation)
162 for Na, F or Cl, when using a beam larger than 15 x 15 $\mu m^2$, and for K when using a beam of
163 50 x 50 $\mu m^2$. However, significant losses were observed for the composition KS3Ax, even
164 when the beam was defocused to 50 μm. For compositions KS3A7.5 and KS3A10, we time-
165 monitored the K loss (counting times from 2 to 20 sec) and extrapolated back to 0 sec to
166 deduce the initial K content. For KS3Ax compositions with $Al_2O_3 \leq 5$mol%, K loss was so
167 significant in the first 5 sec that the extrapolation procedure could not be applied. Data
168 presented in Table 1 for KS3, KS3A2.5 and KS3A5 were calculated, therefore, from the
169 weighing data from the initial starting glass preparation.

170 Raman spectroscopy was employed to examine the structure of the quenched melts.
171 The Raman instrument used is a JASCO model IRS-3100 confocal microRaman spectrometer
172 with holographic gratings. Sample excitation was accomplished with the 532 nm line of a
173 solid-state laser operating at a power of 6.4 mW on the sample. A 50X objective lens was
174 employed for visual microscopic examination and spectroscopic analysis. Signal detection
175 was provided by an Andor Model DV401-F1 1024 x 128 pixel (25 μm pixel size) Peltier-
176 cooled CCD. A grating of 1200 grooves/mm was used, which results in a CCD window
177 covering the 265-2110 $cm^{-1}$ frequency range with resolution of ±3 $cm^{-1}$. Acquisition time was
178 typically 15 min per spectrum.

179 Background correction of the Raman spectra was performed using a cross-validation
180 spline function (Woltring, 1986), fitted to spectral portions devoid of signals near 800 and

181 1300 $cm^{-1}$. After subtraction of the spline function, the 850 to 1300 $cm^{-1}$ region was fitted
182 using 5 to 6 Gaussian peaks with *lmfit* interface (Newville et al. 2014) and the optimization
183 algorithms implemented in the Scipy library (Jones et al. 2001). During fitting, peak half
184 widths were constrained to vary within ±20 $cm^{-1}$ of their initial estimated value and peak
185 frequencies were allowed to vary within ±25 $cm^{-1}$.

186 To avoid the under-constrained problem resulting from the strong convolution of
187 signals from $Q^3$ and $Q^4$ units with similar intensities, we exploit the fact that $Al^{3+}$ enters
188 mostly in fully-polymerized $Q^4$ units in peralkaline compositions (c.f. Mysen et al. 2003;
189 Allwardt et al. 2005; Le Losq et al. 2014). Mysen et al. (2003) showed that addition of Al at
190 constant NBO/T should result in increasing contributions from $Q^4$ units; therefore, we expect
191 little to no change in the half width of the peak assigned to Si-O stretch vibrations in $Q^3$ units
192 (1050-1100 $cm^{-1}$; see Results and Discussion for peak assignments) with increasing Al/(Al +
193 Si) at constant NBO/T. Furthermore, changes of the Na/Si ratio (and polymerization) should
194 not significantly affect the half width of the 1050-1100 $cm^{-1}$ peak assigned to $Q^3$. In the
195 spectra of the $Na_2O$-$SiO_2$ glasses, it is ~32 $cm^{-1}$ for Na/Si = 0.5 (this study), ~27 $cm^{-1}$ for
196 Na/Si = 0.67 (Le Losq et al., 2014) or ~29 $cm^{-1}$ for Na/Si = 1.33 (Neuville 2006). For a given
197 compositional series, we determined the half width of the 1050-1100 $cm^{-1}$ peak in Al-free
198 glasses, typically between 29 and 32 $cm^{-1}$, similar to reported values, and used this value to fit
199 the spectra of Al-bearing glasses.

200 The curve-fitting itself was performed by minimizing the least-square difference
201 between calculated and observed spectra using the Powell optimization algorithm (Powell,
202 1964). After testing all gradient-based and gradient-less optimization algorithms implemented
203 in Scipy, the Powell algorithm (a gradient-less method) gave the most robust and reproducible

fits.

The errors on the estimated peak parameters were determined using the bootstrap method, well established for error estimation in statistics (c.f. Efron and Tibshirani 1994). A three-step bootstrap technique was employed, which consists of (1) resampling the data, accounting for data uncertainty in the model errors; (2) randomly choosing between two optimization algorithms (Powell and Nelder-Mead [Nelder and Mead, 1965]) for fitting the resampled data, accounting for the arbitrariness in the choice of the optimization algorithm and the precision and accuracy of that algorithm, and (3) twice fitting the resampled data with the chosen algorithm. The Nelder-Mead algorithm was chosen as the second algorithm because it provides results that are as robust as those from the Powell algorithm, but its reproducibility is slightly lower. Steps (1), (2) and (3) were repeated $N$ times, and for each parameter, we calculated its standard deviation using its $N$ values from the $N$ models generated by the bootstrap. In this study, we used $N = 128$ because it was found that mean values and standard errors of the fitting parameters did not evolve significantly when $N > 80$.

## RESULTS AND DISCUSSION

In the following sections, F and Cl solubility and solution behavior was determined with glasses. This glass structure reflects the structure of supercooled melt at the glass transition temperature.

### 1. F and Cl solubility in aluminosilicate melts

227 At experimental conditions, F and Cl are released from the thermal decomposition of
228 $AgF_2$ ($AgF_2 \rightarrow Ag_0 + F_2$) and $PdCl_2$ ($PdCl_2 \rightarrow Pd_0 + Cl_2$). At the end of the experiments, $Ag_0$
229 and $Pd_0$ are found as small, shiny beads of metal (nm to 3 μm), as also reported by Jago and
230 Gittins (1989). The presence of these metal beads indicates that Ag and Pd were not oxidized
231 during the experiments and do not bond with the melt structure. As the only volatiles present,
232 F and Cl saturation in the melts is confirmed by the presence of bubbles. In the case of F-
233 bearing samples, these bubbles were nm to 5 μm in diameter, whereas in the Cl-bearing
234 samples, the bubbles were 10 to 40 μm in diameter (Fig.1).

235 The F and Cl concentrations in the silicate and aluminosilicate quenched melts are
236 presented in Table 2 and Table 3. In these analyses, interference of some of the metal beads
237 was unavoidable. The melt compositions were, therefore, renormalized to 100 wt% after
238 subtraction of Ag and Pd contents in the analyses of the melts (up to 6 mol% of Ag and 0.78
239 mol% of Pd). Variation of Ag concentration (from 0 to 6 mol% between individual analytical
240 points) resulted in a change smaller than 0.45 mol% in F, which is near or within one standard
241 deviation of the F analysis. The compositional homogeneity of the quenched melts confirms
242 that a duration of 90 min for the experiments was sufficient to achieve F and Cl equilibrium in
243 melts (Table 2).

244 The F solubility increases from 3.33 (±0.73, 1$\sigma$) to 7.40 (±0.08) mol% in the NS5Ax
245 sodic system, and from 3.63 (±0.23) to 6.52 (±0.55) mol% in the KS5Ax potassic system with
246 increasing Al/(Al + Si) from 0.0 to 0.33 (Fig. 2A). The solubility in NS4Ax and NS5Ax melts
247 is similar, within error. In comparison, in more polymerized melts such as that of $NaAlSi_3O_8$
248 composition [i.e. NBO/T ~ 0; Al/(Al + Si) = 0.25], the F solubility is 6-7 times greater (59
249 mol% F) at the same pressure and temperature conditions (Dingwell 1987).

In contrast to F, Cl solubility is negatively correlated with the bulk Al/(Al + Si) ratio of the melt (Fig. 2B). At 1.5 GPa and 1600ºC, with increasing Al/(Al + Si) from 0 to 0.33, the Cl concentration decreases from 5.70 (± 0.65) to 2.45 (±0.30) mol% in the NS3Ax sodic system, and from 3.63 (± 0.21) down to 1.14 (± 0.20) mol% in the KS3Ax potassic system. The Cl solubility in Na-aluminosilicate melts, therefore, is about 1.5 times higher than that in K-aluminosilicate melts. The Cl solubility NS4Ax (1400ºC) and NS3Ax melts (1600ºC) are comparable (Fig. 2B), suggesting that neither slight changes in Na/Si nor a 200ºC temperature difference significantly affects Cl solubility, the latter observation being in agreement with Stagno and Dolejš (2007), Stelling et al. (2008) and Chevychelov et al. (2008). According to the model of Webster et al. (2015), a 200ºC temperature variation applied to our data should result in a 3% variation in Cl solubility, which is within the standard deviation on the present Cl solubility measurements.

The chlorine data are consistent with those of Zimova and Webb (2006) who also observed decreasing Cl solubility with increasing Al content in $Na_2O$-$Fe_2O_3$-$Al_2O_3$-$SiO_2$ melts. However, they are inconsistent with the empirical Webster et al. (2015) model, which predicts an increase of Cl solubility with Al/(Al + Si). This may arise from the fact that this empirical model was developed on the basis of Cl solubility data in chemically much more complex natural systems. Indeed, results from the model are consistent with a Cl solubility increase from felsic (latite; NBO/T = 0.11; Al/(Al + Si) = 0.25) to mafic (basaltic; NBO/T = 0.76; Al/(Al + Si) = 0.27) melts, as observed by Webster and De Vivo (2002). Therefore, Cl solubility is probably a complex function of the melt composition.

There is a linear, positive relationship between pressure and both F and Cl solubility (Fig. 3). While the F solubility-dependence on pressure is the same regardless of the Al

273 content (Fig. 3A), the Cl solubility-dependence is about three times higher in Al-free and Al-
274 poor (NS3, NS3A5 and KS3, KS3A5) melts than in Al-rich melts (Fig. 3B). Moreover, the
275 pressure dependence of Cl solubility is about three times greater in NS3Ax melts than in
276 KS3Ax melts (Fig. 3B).
277
278 2. Raman spectroscopy of F and Cl-bearing sodic melts
279
280 Raman spectra of volatile-free and of F- or Cl-bearing NS4Ax quenched melts in the
281 frequency range of first order Raman scattering of (Si, Al)-O stretch vibrations are shown in
282 Fig. 4 (between 850 and 1300 $cm^{-1}$). Note that the spectra are reproducible in each sample
283 regardless of the presence and abundance of metal beads. Therefore, we conclude that the
284 presence of metal beads have no influence on the melt structure. There is a maximum between
285 1000 and 1100 $cm^{-1}$ with visible shoulders on both sides, the detailed features of which vary
286 with Al/(Al + Si). This spectral topology resembles the Raman spectra of volatile-free
287 peralkaline aluminosilicate melts (Merzbacher and White 1991; Mysen et al. 2003). However,
288 Raman spectra of F- or Cl-bearing melts differ from spectra of volatile-free melt. In Al-free
289 and Al-poor compositions, both F- and Cl-bearing melts show Raman spectra with more
290 intensity near 950-1000 $cm^{-1}$ and less intensity near 1100 and 1150 $cm^{-1}$ compared to Raman
291 spectra of volatile-free melts. In Al-rich melts, less intensity near 950-1000 $cm^{-1}$ and more
292 intensity near the 1100 and 1150 $cm^{-1}$ are observed in the spectra of both F and Cl-bearing
293 glasses compared to those of volatile-free glasses. In order to decipher those topological
294 differences, Raman spectra were deconvoluted with 5 to 6 bands, in agreement with previous

295 studies on similar melt compositions (Mysen et al., 2003; Le Losq et al., 2014; Dalou and
296 Mysen, 2015).

297 The assignments of bands in the 850-1300 $cm^{-1}$ region of the Raman spectra have been
298 extensively described to be associated with (Si, Al)-O stretch vibrations (e.g. Mysen et al.,
299 1982; McMillan, 1984; Matson et al. 1986; Mysen, 1999; Le Losq et al., 2014). In this study,
300 we assigned the main bands in the 850-890, 930-970, 1070-1110 and 1100-1170 $cm^{-1}$ ranges
301 in accord with Mysen et al. (2003) and Le Losq et al. (2014), who supported the Raman
302 assignments with NMR spectroscopic data. Details on band location, bandwidth and
303 amplitude are presented in Table 4.

304 The band near 950 $cm^{-1}$ (dark grey shading in Fig. 5) is assigned to Si-O stretching
305 vibrations in $Q^2$ structural units, the band near 1100 $cm^{-1}$ (grey shading in Fig. 5) to Si-O
306 stretching vibrations in $Q^3$ units and the bands near 1150 $cm^{-1}$ and 1190 $cm^{-1}$ (white bands in
307 Fig. 5) to stretching of (Si,Al)-O° (O°: bridging oxygen) bonds in $Q^4$ units. Consistent with
308 Mysen et al. (1982), Seifert et al. (1982), Mysen (1990), Neuville and Mysen (1996), Le Losq
309 and Neuville, 2013 and Le Losq et al. (2014), a bimodal shape is observed for the Si-O stretch
310 signal assigned to $Q^4$ units. Two Gaussians, here named $Q^{4,II}$ (1140 $cm^{-1}$) and $Q^{4,I}$ (1170 $cm^{-1}$),
311 are used as a mathematical solution to account for this asymmetry of the Si-O stretch signal
312 from $Q^4$ units (see Le Losq et al. 2014 for further discussion). In contrast, Dalou and Mysen
313 (2015) used only one Gaussian to describe $Q^4$ units; their approach was chosen to facilitate
314 comparison to the data of Mysen (2007). There is, therefore, an expected discrepancy between
315 the Raman fit results of the present study and Dalou and Mysen (2015). However, we chose
316 use two gaussians for fitting the $Q^4$ signal, since it is clearly assymetric in pure silica, silica-
317 rich silicate glasses and tectosilicate glasses. (Mysen et al. 1982; Seifert et al. 1982; Mysen

318 1990; Neuville and Mysen 1996; Le Losq and Neuville 2013; Le Losq et al. 2014; Neuville et
319 al. 2014).

320 A band around 1000-1070 $cm^{-1}$ is observed in all spectra (light grey shading). Results
321 from molecular simulations (Spiekermann et al. 2012; 2013) and comparisons of simulations
322 and neutron scattering data (Sarnthein et al. 1997, Pasquarello et al., 1998) with Raman data
323 (Le Losq and Neuville, 2013; Le Losq et al., 2014) indicate that this peak may be assigned to
324 the Si-O asymmetric stretching vibrational mode of $SiO_2$ tetrahedra. Those studies show that
325 this peak probably arises from asymmetric stretching of Si-O bonds in $Q^n$ units and clearly
326 establish that the Si-O asymmetric stretching mode T2 of $SiO_2$ tetrahedra occur at similar
327 frequencies (Sarnthein et al., 1997; Pasquarello et al., 1998). This band is however difficult to
328 fit, because it is present in a region in the spectra not-well defined, i.e where no significant
329 shoulders or peaks are present. Our results show that its intensity and width increase with
330 increasing Al content, consistently with Le Losq et al. (2014). The width is not significantly
331 changing (±5 $cm^{-1}$), compared to changes observed in tectosilicate glasses (Neuville and
332 Mysen 1996, Le Losq and Neuville 2012).

333 In Raman spectra of Cl-bearing glasses, a band near 890 $cm^{-1}$ was necessary to fit the
334 spectra. It may be assigned to (Si,Al)-$O^-$ ($O^-$: non-bridging oxygen) vibrations in $Q^1$ structural
335 units (c.f. Mysen et al., 1982), but the origin of this peak is uncertain. This peak is barely
336 visible in the spectra, and will be put aside for quantification of the glass polymerization using
337 the area of the $Q^n$ peaks.

338 The curve-fitting of the spectra of F-bearing quenched melts requires an additional
339 band around 990 $cm^{-1}$ (cross-hatched in Fig. 5) to minimize the $\chi^2$ (Table 5). The peak was not
340 observed in spectra of silicate melts with low F content [F/(F+O) ≤ 0.015], but appears at

F/(F+O) > 0.02 (e.g. Mysen and Virgo 1985a; b; Luth 1988b; Mysen et al. 2004). This band is not required in curve-fits of the Raman spectra of halogen-free or Cl-bearing melts. Therefore, it likely can be assigned to a vibration involving F. It may not be assigned to Na-F, because such molecules gives Raman signals near 450-500 $cm^{-1}$ (e.g. Hardy et al. 1969). A band at ~945$cm^{-1}$ was observed in $SiO_2$-F glasses and was assigned to Si-F stretching vibrations in $SiO_3F$ tetrahedral units on the basis of valence force field calculations (Dumas et al. 1982). A peak observed near 907 $cm^{-1}$ was assigned to Si-F stretching vibrations in amorphous fluorinated silicon films (Yamamoto et al. 1983). Fluorine-19 NMR data of F-bearing silicate glasses have provided evidence of $SiO_3F$ and $SiO_2F_2$ complexes, but not of $SiF_4$ and $SiOF_3$ (Duncan et al. 1986). Therefore, the band near 990 $cm^{-1}$ observed in our F-saturated silicate and aluminosilicate melts can be assigned to stretching vibrations of Si-F bonds. In agreement with Dumas et al. (1982), we propose that those bonds occur in $SiO_3F$ tetrahedral units, where fluorine replaces one of the oxygens in the silicate tetrahedral. It is difficult to assess the exact degree of polymerization of the oxygen atoms in the $SiO_3F$ units. Changing the BO/NBO ratio of the $SiO_3F$ units is likely to result in changing the Si-F frequency in such unit (Mysen and Virgo, 1985b). However, we note that the vibrational frequency of the 990 $cm^{-1}$ band is constant, regardless of the Al/(Al + Si) of the present glasses (Table 6). Therefore, the exact extent to which the oxygen forms bridges with neighboring silicate tetrahedra in the $SiO_3F$ units does not change with Al/(Al + Si).

In order to quantify the effect of F and Cl on the silicate melt structure, relative band intensities from the Raman spectra must be converted into $Q^n$-species units fractions through (Mysen, 1990; Mysen and Frantz, 1993)

$$[Q^n] = \theta^n \times A_{Qn} , \quad (1)$$

where $\theta^n$ is a conversion factor, depending directly on the Raman cross section of Si-O bonds in $Q^n$ units. In addition, melt polymerization can be calculated using the mean number of non-bridging oxygen per tetrahedrally coordinated cation (NBO/T; here $Al^{3+}$ and $Si^{4+}$):

$$NBO/T = 2 \times [Q^2] + [Q^3] = 2 \times [\theta^2 \times A_{Q2}] + [\theta^3 \times A_{Q3}] \quad (2a)$$

Comparison of NBO/T between F or Cl-bearing melts and volatile-free melts can be obtained by:

$$\Delta NBO/T = NBO/T_{F \text{ or } Cl} - NBO/T_{Volatile\text{-}free} \quad (2b)$$

The $\theta^2$ and $\theta^3$ values are close to unity for sodium silicates (Mysen, 2007) therefore $\theta^2$ and $\theta^3$ factors are negligible in Eq. 2a. Therefore, we can calculate a Raman-apparent ΔNBO/T with equation 2b with using directly the Raman areas. This Raman-apparent ΔNBO/T will be close to the true ΔNBO/T based on the assumption that $\theta^n$ factors are negligible. Whether or not halogen substitution affects the integrated intensities of Raman bands assigned to Si-O stretch vibrations is not known. By using $\theta^n$-factors determined from halogen-free melts, we might have introduced an unknown inaccuracy in the calculated $Q^n$ fractions in halogen-bearing melts. Although Cl and F may have a slight effect on $\theta^n$ factors, it is not significant enough to influence the rest of the discussion.

## 2.1 F solution mechanisms

### 2.1.1 Fluorine in Al-free melts

385 The F-bearing NS4 silicate glass has fewer $Q^3$ and $Q^4$ and more $Q^2$ units than the
386 halogen-free NS4 glass, which translates to higher Raman-based NBO/T-values (Fig. 6). The
387 dominant complexes in $Na_2O$-$SiO_2$-F melts, inferred from $^{19}F$ and $^{29}Si$ NMR spectroscopy,
388 have been reported to be Na-F complexes (e.g. Schaller et al. 1992; Mysen et al. 2004). The
389 observed depolymerizing effect of F (Fig. 6) is inconsistent with the dominance of (Na+F)-
390 bearing complexes. If this were the only fluorine solution mechanism, the silicate melt would
391 become more polymerized (Raman-based NBO/T decreases). However, the Raman data
392 indicate formation of (Si-F)-bearing complexes, by substitution of F for O.

393 The presence of Si-F bonds were previously reported in $SiO_2$-NaF melts containing >
394 7.5 mol% F (Mysen and Virgo 1985b). In addition, evidence of a small fraction of Si-F in
395 silicate and aluminosilicate melts has been reported from $^{19}F$ NMR spectroscopy (Zeng and
396 Stebbins 2000; Kiczenski et al. 2004; Kiczenski and Stebbins 2006). In a melt with a
397 comparable NBO/T to those of this study (~0.4), Si-F complexes represent 90% of fluoride
398 complexes (Mysen and Virgo, 1985b). Therefore, two competing F solution mechanisms may
399 occur in silicate melts: one involving the formation of M-F complexes, with M being an alkali
400 such as Na or K, and the second being the formation of (Si-F)-bearing complexes:

401 $$2\ \text{Si-O-M} + F_2 \leftrightarrow \text{Si-O-Si} + 2\ \text{M-F} + 1/2O_2\ , \quad (3a)$$

402 $$\text{Si-O-Si} + F_2 \leftrightarrow 2\ \text{Si-F} + 1/2O_2\ . \quad (3b)$$

403 In Eqs. 3a and b, $O_2$ will be released by degassing. Eq. 3a seems to dominate at low F
404 concentrations and results in a polymerization of the glass network, as observed by Mysen et
405 al. (2004; F ~ 3 mol%). In contrast, Eq. 3b appears to be more important at high F
406 concentrations (Mysen and Virgo 1985b; this study), and results in melt depolymerization

(Fig. 6). An equilibrium between Si-F or M-F complexes at a given F concentration may be then described as:

$$\text{Si-F} + \text{Si-O-M} \leftrightarrow \text{M-F} + \text{Si-O-Si} \quad (4)$$

Such an equilibrium reaction is likely dependent on F concentration, melt composition, pressure, and temperature conditions.

### 2.1.2. Fluorine in Al-bearing melts

Fluorine complexes with Al-F and Na-F bonding have been reported as the dominant solution mechanisms of F in anhydrous aluminosilicate melts (e.g. Schaller et al. 1992; Zeng and Stebbins 2000; Mysen et al. 2004; Baasner et al. 2014). The Al-F/Na-F abundance ratio increases with increasing Al/(Al + Si) of the melt (Mysen et al. 2004), which is consistent with increasing F solubility with increasing Al/(Al + Si) (Fig. 2). This is also consistent with the decreasing Raman signal assigned to Si-F bonds with increasing Al/(Al + Si) (Table 6). Therefore, in addition to fluorine reacting with Si-O-Si and Si-O-M bonds through the mechanisms described by Eqns. 3 and 4, F also can react with Si-O-Al bonds in aluminosilicate melts as:

$$\text{Si-O-Al} + F_2 \leftrightarrow \text{Si-F} + \text{Al-F} + 1/2O_2\ , \quad (5a)$$

$$2\ \text{Si-O-Al} + F_2 \leftrightarrow \text{Si-O-Si} + 2\ \text{Al-F} + 1/2O_2\ . \quad (5b)$$

As a result, in addition of Eq. 4, two additional equilibria may exist between Si-F, Al-F and M-F complexes:

$$\text{M-F} + \text{Si-O-Al} \leftrightarrow \text{Si-O-M} + \text{Al-F}, \quad (6a)$$

$$\text{Si-F} + \text{Si-O-Al} \leftrightarrow \text{Si-O-Si} + \text{Al-F}. \quad (6b)$$

If $Al^{3+}$ and its surrounding O and F atoms form fully neutral molecular species, Eqs. 5a and b may also imply that the alkali metals (here $Na^{+}$ or $K^{+}$), which were charge compensating $Al^{3+}$ in tetrahedral coordination, become network modifiers. Consequently, Eqs. 5a and b may result in network depolymerization, potentially explaining increasing $Q^2$ and $Q^3$ fractions upon F addition in aluminosilicate glasses (Fig. 6).

The equilibrium constants of the above equations are unknown. However, existing data suggest that equilibria for solution mechanisms presented in Eq. 3a, 3b and 5a and b depend mostly on pressure (Fig. 2) and Al/(Al + Si) ratio (Fig. 3). The comparison of the various existing data reported above indicate that Eqs. 4a, 4b, 6a and 6b, which define the coexistence of the various F-bearing complexes in the melt, have equilibrium constants depending on F concentration, melt chemical composition, and possibly temperature. Dalou and Mysen (2015) also show that Si-F complexes increase with increasing $H_2O$ content dissolved in aluminosilicate melts.

## 2.2 Cl solution mechanisms

### 2.2.1 Chlorine in Al-free melts

It has been previously suggested that Cl dissolves in silicate melts by forming Cl-bearing complexes that contain Cl preferentially bonded to network-modifiers (Ca, Na or K; e.g. Stebbins and Du 2002; Sandland et al. 2004; Zimova and Webb 2006; Evans et al. 2008; Baasner et al. 2013). Such a mechanism means that in Na-silicate melts, for example,

452 formation of NaCl complexes results in a decrease in abundance of network-modifying $Na^+$,
453 which results in silicate melt polymerization:

454 $$Si\text{-}O\text{-}Na + Cl_2 \leftrightarrow 2\ Si\text{-}O\text{-}Si + 2NaCl + 1/2O_2 \quad (7)$$

455 Analogous expressions can be written for other alkali metals and alkaline earths.

456 However, the Raman-based NBO/T of the C5NS4 glass is 0.32 higher than that of the
457 pure NS4 glass (Table 6). The fractions of $Q^4$ and $Q^3$ decrease slightly and that of $Q^2$
458 increases in the C5NS4 glass compared to the pure NS4 glass (Table 6, Fig. 6). Moreover, an
459 additional Raman peak is observed in the Cl-bearing glass near 890 $cm^{-1}$, which may be
460 assigned to (Si,Al)-$O^-$ vibrations in $Q^1$ structural units (c.f. Mysen et al., 1982 and references
461 therein). This peak does not contribute significantly to spectra (Fig. 5), but its appearance, as
462 well as the increase of $Q^2$ fraction suggests an increase of melt depolymerization upon Cl
463 solution.

464

465 2.2.2 Chlorine in Al-bearing melts

466

467 By increasing Al/(Al + Si) of Cl-saturated melts, $Q^3$ fraction decreases, whereas $Q^4$
468 fraction increases and $Q^2$ fraction remains constant, within error (Table 6, Fig. 6). In other
469 words, Cl has a polymerizing effect in aluminosilicate melts. This effect increases with melt
470 Al/(Al + Si) ratio (Fig. 6). This behavior can be explained with the aid of NaCl complexes, as
471 described by Eq. 7. As the melt Al/(Al + Si) increases, the bulk $Q^3$ fraction decreases (Fig. 6),
472 and the solubility of Cl also decreases (Fig. 2). In addition, the ionic radius of alkali metals
473 affects the solubility of Cl at a given Al/(Al + Si) ratio (Figs. 2, 3). This suggests a control of

474 the Cl solution behavior, and hence solubility, by the properties of network modifier metals
475 together with their interaction with specific $Q^n$ units.

476 Sandland et al. (2004), using $^{35}Cl$ NMR, estimated that up to 10% of the dissolved
477 chlorine was in the form of Al-Cl or Si-Cl bonding in aluminosilicate melts. Although it
478 cannot be asserted with certainty, we found no evidence of Si-Cl bonding in either Al-free or
479 in Al-bearing melts.

480

481 IMPLICATIONS

482

483 Both the solubility of F and Cl in melts and their effect on melt structure are governed by the
484 type of complexes formed with these halogens. The different solubility behavior (Fig. 2) may
485 be related preferential bonding of F with Al and Si at high F concentration through Eqs. 3b, 5a
486 and b, whereas Cl mainly bonds with network-modifying alkali cations. This difference also
487 explains why Cl is more sensitive than F to the type of alkali (Na or K) in the melt (Fig. 2),
488 although it remains unclear why Cl is more soluble in sodic systems than in potassic systems.
489 It has been suggested that higher field strength cations ($Na^+ > K^+$) form more stable bonding
490 with $Cl^-$ (Stebbins and Zeng 2000). This behavior is consistent with Cl diffusivity data for
491 phonolitic melts (Balcone-Boissard et al. 2009), which suggest that Cl interacts more strongly
492 with Na than with K.

493 In Al-free melts, F and Cl have comparable solubility (within error, Fig. 2). In those
494 melts, F causes depolymerization of the silicate structure, via formation of Si-F complexes.
495 The chlorine solution mechanism seems also to cause depolymerization; the addition of Cl to
496 silicate glass results an increase of Raman-based NBO/T and in the formation of highly

497 depolymerized $Q^1$ and $Q^2$ units within the silicate network. The exact nature of the bonding of
498 Cl in the present silicate melt remains unknown, but it is probable that Cl atoms reside in
499 close proximity of the formed $Q^1$ and $Q^2$ units, where alkali metals will also be concentrated.
500 The addition of Al to silicate melts results in different relationships between dissolved
501 halogen and aluminosilicate melt structure. Fluorine can react with the various Si-O-M Si-O-
502 Si and Si-O-F bonds through different reactions with their equilibrium constants affected by
503 the Al/(Al + Si) ratio of the melt, for instance. Indeed, the effect of F on the aluminosilicate
504 melt structure depends primarily on the Na/Al ratio of the melt (Dingwell and Scarfe 1985;
505 Dingwell 1989; Mysen et al. 2004), which determines the (Si,Al)-F/Na-F ratio. In contrast, Cl
506 complexes mostly with network-modifiers, leading to melt polymerization. The effect of Cl
507 on melt structure seems to rely mostly on its affinity to a specific alkali or alkali-earth cation,
508 partly driving its solubility (Fig. 2).
509 It follows from the solution mechanisms of F and Cl that their effects on melt structure
510 increase with Al/(Al + Si) content of magmas (Fig. 6). In terms of magma properties, this
511 implies that the effect of F on magma viscosity increases from basaltic to felsic compositions.
512 Furthermore, because several wt% F is soluble in Al-rich magma, fluorine can cause viscosity
513 reduction of up to several orders of magnitude (as measured by Baasner et al. 2013), making it
514 as efficient as $H_2O$ in this regard (Dingwell and Mysen 1985). In contrast, Cl solubility
515 decreases with increasing degree of magma differentiation [increasing Al/(Al + Si)]. Its
516 influence on the rate of change of NBO/T with Al/(Al + Si) is smaller, therefore, than for F-
517 bearing magma. It follows therefore that any magma property that depends on melt
518 polymerization (e.g., viscosity, compressibility, element partitioning) is more sensitive to
519 Al/(Al + Si) in F-rich magmatic systems than in Cl-rich systems. This is also observed in

hydrous aluminosilicate melts in which $H_2O$ melt depolymerization is more enhanced by F addition than by Cl addition (Dalou and Mysen 2015).

The effect of Cl on magma properties, however, does not simply depend on Al/(Al + Si) content. For example, Webb et al. (2014) show that Cl decreases the viscosity of iron-bearing aluminosilicate melts, whereas it increases the viscosity of iron-free aluminosilicate melts. This shows that the electronic properties of network former and network modifier elements play a strong role in determining the formation and stability of $M^{x}_{1/x}Cl$ complexes (with M a modifier element and x its electronic charge) within the silicate melt. This is corroborated by literature data that shows the influences of the molar $(Al_2O_3/(CaO+Na_2O+K_2O))$, $(Na_2O/(Na_2O+K_2O))$, and (Ca+Mg)/(Na+K) ratios of melts on the efficiency of Cl dissolution at fixed pressure conditions (Métrich and Rutherford 1992; Chevychelov and Chevychelova 1997; Signorelli and Carroll 2000). From an extension of these relationships, Webster et al. (2015) compared the Cl solubility of fluid-saturated melts with increasing concentration of $(Ca^{1/2} + Mg^{1/2} + Al^{1/2} + Na)$ and decreasing Si concentration in the melt for a range of *P-T* conditions. A very good agreement is found between Webster et al. (2015) model data and our experimental data of Cl solubility in Al-free melts with pressure.

From the above results and interpretations, it follows that the pressure (depth) at which halogens (both Cl and F) will be exsolved from a magmatic liquid is sensitive to the magma composition. For example, Al-rich magmas are likely to exsolve greater amounts of Cl than Al-poor magmas (Fig. 2 and 3). Consistently, Chevychelov and Suk (2003) have demonstrated that Cl solubility decreases by an order of magnitude as basaltic melts evolve to felsic compositions and that Cl partitions increasingly in favor of fluids as magmas evolve

543 from mafic to felsic residual melt compositions.

544

545 ACKNOWLEDGMENTS

546

547 This research was conducted with partial support from NSF grant EAR- 1212754 (to
548 B.O.M. and C.D.), and NAI grant to the Geophysical Laboratory. We acknowledge very
549 helpful reviews by A.E. Grant Henderson, Hélène Balcone-Boissard and one anonymous
550 reviewer, which considerably improve this manuscript. We thank Robert Dennen for his help
551 with English edits. We also thank J.T. Armstrong and K. Crispin for their help with the
552 optimization of the SEM/EDS analytical protocol.

553

554 REFERENCES

555

556 Baasner, A., Schmidt, B.C., and Webb, S.L. (2013) Compositional dependence of the
557 rheology of halogen (F, Cl) bearing-aluminosilicate melts. Chemical Geology, 346(C),
558 172-183.
559 Baasner, A., Hung, I., Kemp, T.F., Dupree, R., Schmidt, B.C., and Webb, S.L. (2014)
560 Constraints on the incorporation mechanism of chlorine in peralkaline and peraluminous
561 $Na_2O$-CaO-$Al_2O_3$-$SiO_2$ glasses. American Mineralogist, 99(8-9), 1713-1723.
562 Balcone-Boissard, H., Baker, D.R., Villemant, B., and Boudon, G. (2009) F and Cl diffusion
563 in phonolitic melts: Influence of the Na/K ratio. Chemical Geology, 263, 89-98.
564 Balcone-Boissard, H., Boudon, G. and Villemant, B. (2011) Textural and geochemical
565 constraints on eruptive style of the 79 AD eruption at Vesuvius. Bulletin of Volcanology,

73, 279-294.

Bohlen, S.R. (1984) Equilibria for precise pressure calibration and a frictionless furnace assembly for the piston-cylinder apparatus. Neues Jahrbuch für Mineralogie, Mh., 84, 404-412.

Boyd, F.R. and England, J.L. (1960) Apparatus for phase equilibrium measurements at pressures up to 50 kilobars and temperatures up to 1750°C. Journal of Geophysical Research, 65, 741-748.

Chevychelov, V.Y., and Suk, N.I. (2003) Influence of the composition of magmatic melt on the solubility of metal chlorides at pressures of 0.1-3.0 kbar. Petrology. 11, 62-74.

Chevychelov, V.Y., and Chevychelova, T.K. (1997) Partitioning of Pb, Zn, W, Mo, CI, and major elements between aqueous fluid and melt in the systems granodiorite (granite, leucogranite)-$H_2O$-NaCl-HCl. Neues Jahrbuch für Mineralogie-Abhandlungen, 101-115.

Chevychelov, V.Y., Bocharnikov, R.E., and Holtz, F. (2008) Experimental study of chlorine and fluorine partitioning between fluid and subalkaline basaltic melt. Doklady Earth Sciences, 422(1), 1089-1092.

Dingwell, D.B. (1987) Melt viscosities in the system $NaAlSi_3O_8$-$H_2O$-$F_2O^{-1}$. (B.O. Mysen, Ed.) (pp. 423-432). Magmatic Processes: Physicochemical Principles.

Dingwell, D.B. (1989) Effect of fluorine on the viscosity of diopside liquid. American Mineralogist, 74, 333-338.

Dingwell, D.B., and Hess, K.U. (1998) Melt viscosities in the system Na-Fe-Si-O-F-Cl: Contrasting effects of F and Cl in alkaline melts. American Mineralogist, 83, 1016-1021.

587 Dingwell, D.B., and Mysen, B.O. (1985) Effects of water and fluorine on the viscosity of
588 albite melt at high pressure: a preliminary investigation. Earth and Planetary Science
589 Letters, 74(2), 266-274.
590 Dingwell, D.B., and Scarfe, C.M. (1985) Chemical diffusion of fluorine in melts in the system
591 $Na_2O$-$Al_2O_3$-$SiO_2$. Earth and Planetary Science Letters, 73, 377-384.
592 Dingwell D.B., Knoche R., and Webb S.L. (1993) The effect of F on the density of
593 haplogranite melt. American Mineralogist, 78, 325-330
594 Dumas, P., Corset, J., Carvalho, W., Levy, Y., Neuman, Y. (1982) Fluorine-doped vitreous
595 silicate analysis of fiber optics preforms by vibrational spectroscopy. Journal of Non-
596 Crystalline Solids, 47, 239-242.
597 Duncan T.M., Douglass D.C., Csenscits R., and Walker K.L. (1986) Study of fluorine in
598 silicate glasses with $^{19}F$ nuclear magnetic resonance spectroscopy. Journal of Applied
599 Physics, 60, 130-136.
600 Evans, K.A., Mavrogenes, J.A., O'Neill, H.S., Keller, N.S., and Jang, L.Y. (2008) A
601 preliminary investigation of chlorine XANES in silicate glasses. Geochemistry
602 Geophysics Geosystems, 9(10), Q10003, doi:10.1029/2008GC002157
603 Efron, B. and Tibshirani, R. (1994) An introduction to the Bootstrap. Monographs on
604 Statistics and Applied Probability 57, Chapman & Hall/CRC.
605 Filiberto, J., and Treiman, A.H. (2009) The effect of chlorine on the liquidus of basalt: First
606 results and implications for basalt genesis on Mars and Earth. Chemical Geology, 263(1-
607 4), 60–68. doi:10.1016/j.chemgeo.2008.08.025
608 Filiberto, J., Wood, J., Dasgupta, R., Shimizu, N., Le, L., and Treiman, A.H. (2012) Effect of
609 fluorine on near-liquidus phase equilibria of an Fe–Mg rich basalt. Chemical Geology,

312-313(C).

Foley S. F., Taylor W. R., and Green D. H. (1986) The effect of fluorine on phase relationships in the system $KAlSiO_4$-$Mg_2SiO_4$-$SiO_2$ at 28 kbar and the solution mechanism of fluorine in silicate melts. Contributions to Mineralogy and Petrology, 93, 46-55.

Giordano, D., Romano, C., Dingwell, D.B., Poe, B., and Behrens, H. (2004) The combined effects of water and fluorine on the viscosity of silicic magmas. Geochimica et Cosmochimica Acta, 68(24), 5159-5168.

Giordano, D., Russell, J.K., and Dingwell, D.B. (2008) Viscosity of magmatic liquids. Earth and Planetary Science Letters, 271, 123-134.

Jago, B.C., and Gittins, J. (1989) Silver fluoride (AgF) as source of fluorine in experimental petrology. American Mineralogy, 74, 936-937.

Jones E., Oliphant, E., Peterson, P., et al. (2001) SciPy: Open Source Scientific Tools for Python. http://www.scipy.org/

Kiczenski, T.J., Du, L.S., and Stebbins, J.F. (2004) F-19 NMR study of the ordering of high field strength cations at fluoride sites in silicate and aluminosilicate glasses. Journal of non-crystalline solids, 337(2), 142-149.

Kiczenski, T.J., and Stebbins, J.F. (2006) The effect of fictive temperature on the structural environment of fluorine in silicate and aluminosilicate glasses. Journal of the American Ceramic Society, 89(1), 57-64.

Kohn, S.C., Dupree, R., Mortuza, M.G., and Henderson, C.M.B. (1991). NMR evidence for five- and six- coordinated aluminum fluoride complexes in F-bearing aluminosilicate glasses. American Mineralogist, 76, 309-312.

633 Kuisma-Kurkula, P. (2000) Accuracy, precision and detection limits of SEM-WDS, SEM-
634 EDS and PIXE in the multi-elemental analysis of medieval glass. X-Ray Spectrometry,
635 29, 111-118.
636 Kushiro, I. (1976) A new furnace assembly with a small temperature gradient in solid-media,
637 high-pressure apparatus. Carnegie Institution Washington year Book, 75, 832-833.
638 Lasaga, A.C. (1982). Optimization of CNOD for molecular orbital calculation on silicates.
639 Physics and chemistry of minerals, 8, 36-46.
640 Laughlin, R.B., and Joannopoulos, J.D. (1977) Phonons in amorphous silica. Physical Review
641 B, 16(6), 2942.
642 Le Losq, C., and Neuville, D.R. (2013) Effect of the Na/K mixing on the structure and the
643 rheology of tectosilicate silica-rich melts. Chemical Geology, 346, 57-71.
644 Le Losq, C., Neuville, D.R., Florian, P., Henderson, G.S., and Massiot, D. (2014) The role of
645 $Al^{3+}$ on rheology and structural changes in sodium silicate and aluminosilicate glasses
646 and melts. Geochimica et Cosmochimica Acta, 126, 495-517.
647 Luth R.W. (1988a) Effects of F on phase equilibria and liquid structure in the system
648 $NaAlSiO_4$-$CaMgSi_2O_6$-$SiO_2$. American Mineralogist, 73, 306-312.
649 Luth, R.W. (1988b) Raman spectroscopic study of the solubility mechanisms of F in glasses
650 in the system CaO-$CaF_2$-$SiO_2$. American Mineralogist, 73, 297-305.
651 Matson, D.W., Sharma, S.K., and Philpotts, J.A. (1986) Raman spectra of some tectosilicates
652 and of glasses along the orthoclase-anorthite and nepheline-anorthite joins. American
653 Mineralogist, 71, 694-704.
654 McMillan, P. (1984) A Raman spectroscopic study of glasses in the system CaO-MgO-
655 $SiO_2$. American Mineralogist, 69, 645-659.

656 Merzbacher, C.I., and White, W.B. (1991) The structure of alkaline earth aluminosilicate
657 glasses as determined by vibrational spectroscopy. Journal of Non-Crystalline Solids,
658 130, 18-34.
659 Métrich, N., and Rutherford, M.J. (1992) Experimental study of chlorine behavior in hydrous
660 silicic melts. Geochimica et Cosmochimica Acta, 56(2), 607-616.
661 Mysen, B.O. (2007) The solution behavior of $H_2O$ in peralkaline aluminosilicate melts at high
662 pressure with implications for properties of hydrous melts. Geochimica et Cosmochimica
663 Acta, 71(7), 1820-1834.
664 Mysen, B.O. (1999) Structure and properties of magmatic liquids: From haplobasalt to
665 haploandesite. Geochimica et Cosmochimica Acta, 63(1), 95-112.
666 Mysen, B.O. (1990) Relationships between silicate melt structure and petrologic
667 processes. Earth-Science Reviews, 27(4), 281-365.
668 Mysen, B.O., and Cody, G.D. (2005) Solution mechanisms of $H_2O$ in depolymerized
669 peralkaline melts. Geochimica et Cosmochimica Acta, 69(23), 5557-5566.
670 Mysen, B.O., and Richet, P. (2005) Silicate Glasses and Melts, Properties and Structure.
671 Elsevier, Amsterdam.
672 Mysen, B.O., and Cody, G.D. (2001) Silicate-phosphate interactions in silicate glasses and
673 melts: II. Quantitative, high-temperature structure of P-bearing alkali aluminosilicate
674 melts. Geochimica et Cosmochimica Acta, 65(14), 2413-2431.
675 Mysen, B.O., and Frantz, J.D. (1993) Structure of silicate melts at high temperature: In-situ
676 measurements in the system $BaO$-$SiO_2$ at 1669ºC. American Mineralogist, 78, 699-709.
677 Mysen, B.O., and Virgo, D. (1985a) Structure and properties of fluorine-bearing
678 aluminosilicate melts: the system $Na_2O$-$AI_2O_3$-$SiO_2$-F at 1 atm. Contributions to

679 Mineralogy and Petrology, 91, 205-220.

680 Mysen, B.O., and Virgo, D. (1985b). Interaction Between Fluorine and Silica in Quenched
681 Melts on the Joins $SiO_2$-$AlF_3$ and $SiO_2$- NaF Determined by Raman Spectroscopy.
682 Physics and chemistry of minerals, 12, 77-85.

683 Mysen, B.O., Cody, G.D., and Smith, A. (2004) Solubility mechanisms of fluorine in
684 peralkaline and meta-aluminous silicate glasses and in melts to magmatic temperatures.
685 Geochimica et Cosmochimica Acta, 68(12), 2745-2769.

686 Mysen, B.O., Lucier, A., and Cody, G.D. (2003) The structural behavior of $Al^{3+}$ in peralkaline
687 melts and glasses in the system $Na_2O$-$Al_2O_3$-$SiO_2$. American Mineralogist, 88, 1668-
688 1678.

689 Mysen, B.O., Finger, L.W., Virgo, D., and Seifert, F.A. (1982) Curve-fitting of Raman
690 spectra of silicate glasses. American Mineralogist, 67, 686-695.

691 Nelder, J.A. and Mead, R. (1965) A simplex method for function minimization. Computer
692 Journal, 7, 308-313.

693 Neuville, D.R. (2006) Viscosity, structure and mixing in (Ca, Na) silicate melts. Chemical
694 Geology, 229, 28-41.

695 Neuville, D.R., and Mysen, B.O. (1996) Role of aluminium in the silicate network: In situ,
696 high-temperature study of glasses and melts on the join $SiO_2$-$NaAlO_2$. Geochimica et
697 Cosmochimica Acta, 60(10), 1727-1737.

698 Neuville, D. R., Hennet, L., Florian, P., and de Ligny, D. (2014) In situ high-temperature
699 experiments. Reviews in Mineralogy and Geochemistry, 78(1), 779-800.

700 Newville, M., Stensitzki, T., Allen, D.B. and Ingargiola, A. (2014) LMFIT: Non-Linear Least-
701 Square Minimization and Curve-Fitting for Python. Zenodo. 10.5281/zenodo.11813

Osborn E.F, and Muan A. (1960) Phase equilibrium diagrams for ceramists. Plate 4. The system $Na_2O$-$Al_2O_3$-$SiO_2$. American Ceramic Society, Columbus, OH.

Pasquarello, A., Sarnthein, J., and Car, R. (1998) Dynamic structure factor of vitreous silica from first principles: Comparison to neutron-inelastic-scattering experiments. Physical Review B, 57(22), 14133.

Piriou, B., and McMillan, P. (1983) Vibrational spectroscopy of silicates and the order problem. Bulletin de Mineralogie, 106(1-2), 23-32.

Powell, M.J.D. (1964). An efficient method for finding the minimum of a function of several variables without calculating derivatives. Computer Journal, 7(2), 155-162.

Raudsepp, M. (1995) Recent advances in the electron micro-analysis of minerals for the light elements. The Canadian Mineralogist, 33, 203-218.

Sandland, T.O., Du, L.-S., Stebbins, J. F., and Webster, J. D. (2004) Structure of Cl-containing silicate and aluminosilicate glasses: A $^{35}$Cl MAS-NMR study. Geochimica et Cosmochimica Acta, 68(24), 5059-5069.

Sarnthein, J., Pasquarello, A., and Car, R. (1997) Origin of the high-frequency doublet in the vibrational spectrum of vitreous $SiO_2$. Science, 275(5308), 1925-1927.

Sato, R.K., McMillan, P.F., Dennison, P., and Dupree, R. (1991) Structural investigation of high alumina glasses in the CaO-AlO-SiO system via Raman and magic angle spinning nuclear magnetic resonance spectroscopy. Physics and Chemistry of Glasses, 32(4), 149-156.

Schaller, T., Dingwell, D.B., Keppler, H., Knöller, W., Merwin, L., and Sebald, A. (1992) Fluorine in silicate glasses: A multinuclear nuclear magnetic resonance study. Geochimica et Cosmochimica Acta, 56, 701-707.

Seifert, F., Mysen, B.O., and Virgo, D. (1982) Three-dimensional network structure of quenched melts (glass) in the systems $SiO_2$-$NaAlO_2$, $SiO_2$-$CaAlO_4$ and $SiO_2$-$MgAl_2O_4$. American Mineralogist, 67, 696-717.

Sharma, S.K., and Simons, B. (1981) Raman study of crystalline polymorphs and glasses of spodumene composition quenched from various pressures. American Mineralogist, 66(1-2), 118-126.

Signorelli, S., and Carroll, M.R. (2000) Solubility and fluid-melt partitioning of Cl in hydrous phonolitic melts. Geochimica et Cosmochimica Acta, 64(16), 2851-2862.

Signorelli, S., and Carroll, M.R. (2002) Experimental study of Cl solubility in hydrous alkaline melts: constraints on the theoretical maximum amount of Cl in trachytic and phonolitic melts. Contributions to Mineralogy and Petrology, 143(2), 209-218.

Spiekermann, G. and Steel-McInnis, M. and Schmidt, C. and Jahn, S. (2012) Vibrational mode frequencies of silica species in $SiO_2$-$H_2O$ liquids and glasses from ab initio molecular dynamics. The Journal of Chemical Physics, 136, 154501.

Spiekermann, G. and Steele-MacInnis, M. and Kowalski, P. M. and Schmidt, C. and Jahn, S. (2013) Vibrational properties of silica species in MgO-$SiO_2$ glasses obtained from ab initio molecular dynamics. Chemical Geology, 346, 22-33.

Stagno, V., and Dolejš, D. (2007) Chlorine solubility in polymerized aluminosilicate melts. Bayerisches Geoinstitut Annual Report 2007. 137-140.

Stebbins, J.F., and Zeng, Q. (2000) Cation ordering at fluoride sites in silicate glasses: a high-resolution 19F NMR study. Journal of Non-Crystalline Solids, 262(1-3), 1-5.

Stebbins, J.F., and Du, L.-S. (2002) Chloride ion sites in silicate and aluminosilicate glasses: A preliminary study by $^{35}Cl$ solid-state NMR. American Mineralogist, 87, 359-363.

748 Stebbins, J.F., Kroeker, S., and Lee, S.K. (2000) Quantification of five- and six-coordinated
749 aluminum ions in aluminosilicate and fluoride-containing glasses by high-field, high-
750 resolution $^{27}$Al NMR. Journal of Non-Crystalline Solids, 275, 1-6.
751 Stelling, J., Botcharnikov, R.E., Beermann, O., and Nowak, M. (2008) Solubility of $H_2O$ and
752 chlorine-bearing fluids in basaltic melt of Mount Etna at *T*= 1050-1250° C and *P*= 200
753 MPa. Chemical Geology,256(3), 102-110.
754 van Groos, A.F.K., and Wyllie, P.J. (1968) Melting Relationships in the System $NaAlSi_3O_8$-
755 NaF-$H_2O$ to 4 Kilobars Pressure. The Journal of Geology, 76(1), 50-70.
756 Villemant, B., and Boudon, G. (1998) Transition from dome-forming to plinian eruptive styles
757 controlled by $H_2O$ and Cl degassing. Nature, 392(6671), 65-69.
758 Webster, J.D. (2004) The exsolution of magmatic hydrosaline chloride liquids. Chemical
759 geology, 210 (1-4), 33-48.
760 Webster, J.D., and De Vivo, B. (2002) Experimental and modeled solubilites of chlorine in
761 aluminosilicate melts, consequences of magma evolution, and implications for exsolution
762 of hydrous chloride melt at Mt. Somma-Vesuvius. American Mineralogist, 87, 1046-
763 1061.
764 Woltring, H.J. (1986) A FORTRAN package for generalized, cross-validator spline
765 smoothing and differentiation. Advances in Engineering Software, 8(2), 104-113.
766 Wyllie, P.J., and Tuttle, O.F. (1961) Experimental investigation of silicate systems containing
767 two volatile components. American Journal of Science, 259, 128-143.
768 Yamamoto K., Nakanishi T., Kasahara H., and Abe K. (1983) Raman scattering of SiF4
769 molecules in amorphous fluorinated silicon., Journal of Non-Crystalline Solids, 59-60,
770 213-216.

771 Zeng, Q., and Stebbins, J.F. (2000) Fluoride sites in aluminosilicate glasses: High-resolution
772 19F NMR results. American Mineralogist, 85, 863-867.
773 Zimova, M. and Webb, S.L. (2006) The effect of chlorine on the viscosity of $Na_2O$-$Fe_2O_3$-
774 $Al_2O_3$-$SiO_2$ melts. American Mineralogist, 91(2-3), 344-352.
775 Zimova, M., and Webb, S.L. (2007). The combined effects of chlorine and fluorine on the
776 viscosity of aluminosilicate melts. Geochimica et Cosmochimica Acta,71(6), 1553-1562.
777
778 FIGURE CAPTIONS
779
780 Figure 1. Back-scattered electron image of C5NS3A5 sample. Chlorine-saturation is indicated
781 by the presence of bubbles from 5 to 35 μm in diameter. Traces of alumina suspension used
782 for polishing are observed within the bubbles. Small white dots (< 5μm) are $Pd_0$ drops from
783 the $PdCl_2 \rightarrow Pd_0 + Cl_2$ decomposition. Fluorine samples look similar to chlorine samples,
784 except that bubbles in F-bearing samples are smaller (nm to 5 μm in diameter) than in Cl-
785 bearing samples.
786
787
788 Figure 2. Solubility in mol% of F (A) and Cl (B) in aluminosilicate quenched melts as a
789 function of their bulk Al/(Al + Si). All samples were equilibrated at 1.5 GPa. Samples
790 F10NS5Ax, F10NS4Ax, F10KS5Ax and C5NS4Ax were synthesized at 1400ºC and samples
791 C5NS3Ax and C5KS3Ax were synthesized at 1600ºC. Error bars represent one standard
792 deviation of the average of analyses of each sample (number of analysis are shown in brackets
793 in Table 2.). For F solubility experiments, diamonds refer to NS5Ax and NS4Ax samples and

794 triangles to KS5Ax. For Cl-solubility experiments, circles refer to NS3Ax and NS4Ax
795 samples and reversed triangles are KS3Ax samples. The grey scale represents the variation of
796 the bulk melt Al/(Al + Si) ratio. The same color code is used in Figs. 3 and 7. Large symbols
797 are for NS4Ax samples measured by Raman spectroscopy and presented in Figs. 3 and 7.
798
799 Figure 3. Solubility variation of F (A) and Cl (B) as a function of pressure. Symbols are the
800 same as in Fig. 2. Solid lines show F and Cl solubility dependence in the sodic systems, and
801 dashed lines in the potassic systems. Samples NS5Ax, KS5Ax and NS4Ax were synthesized
802 at 1400ºC and samples NS3Ax and KS3Ax at 1600ºC. Both F and Cl solubility increase with
803 increasing pressure from 1.0 to 2.5 GPa. The relation of Cl solubility with pressure appears to
804 depend on melt composition as shown by the Cl vs pressure slopes varying with the bulk melt
805 Al/(Al + Si) ratio. In contrast, the F solubility dependence with pressure does not vary, or not
806 significantly, with the bulk melt Al/(Al + Si) ratio, but its dependence is higher in the potassic
807 system than in the sodic systems.
808
809 Figure 4. Raman spectra between 850 and 1300 $cm^{-1}$ obtained for volatile-free samples (in
810 grey) and in volatile-bearing (F- and Cl-bearing) samples (in black). Spectra, volatile-free or
811 volatile-bearing, are normalized to have the same area.
812
813 Figure 5. Examples of curve-fitted Raman spectra of melts in the frequency region of (Si, Al)-
814 O stretch vibrations for compositions indicated on each plot. The spectra are normalized to
815 100% intensity. The individual lines are of Gaussian shape and fitted to the spectra as
816 discussed in the text. Peaks near 900, 950, 1100, 1150 and 1180 $cm^{-1}$ Raman spectra are

817 related to (Si, Al)-O stretching in $Q^2$, $Q^3$, $Q^{4,II}$ and $Q^{4,I}$ tetrahedral units. See text for discussion
818 of band assignments. The 1000-1070 $cm^{-1}$ peak is related to the stretching $T_{2S}$ vibrational
819 mode of $SiO_2$ units as explained in the test.
820
821 Figure 6. Relative area of the Raman signals assigned to A. $Q^2$, $A_{Q2}$; B. $Q^3$, $A_{Q3}$; and C. $Q^4$,
822 $A_{Q4}$, structural units of volatile-free (squares), F-bearing (diamonds) and Cl-bearing samples
823 (circles). and D. Variation of melt polymerization, ΔNBO/T, with the addition of F and Cl, as
824 a function of the bulk melt Al/ (Al + Si) ratio. Increasingly darker symbols represent
825 increasing Al/(Al + Si). Unit fractions of $Q^n$ and ΔNBO/T are presented in Table 4.
826
827
828
829
830
831
832
833
834 TABLES
835
836
837 Table 1: Composition of starting glasses (wt%)[a]

838

| | NS3A0 [13] | NS3A2.5 [16] | NS3A5 [12] | NS3A7.5 [13] | NS3A10 [12] | NS3A12.5 [18] |
|---|---|---|---|---|---|---|
| | $PdCl_2$ | $PdCl_2$ | $PdCl_2$ | $PdCl_2$ | $PdCl_2$ | $PdCl_2$ |
| $SiO_2$ | 75.96(57) | 69.90(20) | 64.98(62) | 57.89(45) | 52.41(31) | 46.80(43) |
| $Al_2O_3$ | ---- | 4.55(6) | 7.84(10) | 12.08(13) | 15.86(19) | 18.99(28) |
| $Na_2O$ | 23.75(70) | 26.31(15) | 28.06(28) | 30.90(32) | 32.09(37) | 33.95(33) |
| Total | 99.71 | 100.77 | 100.89 | 100.87 | 100.36 | 99.74 |
| Al/(Al + Si)[b] | 0 | 0.07(0.3) | 0.12(1) | 0.20(1) | 0.26(1) | 0.32(1) |
| NBO/T[c] | 0.61 | 0.61 | 0.61 | 0.63 | 0.61 | 0.63 |
| | NS5A0 [12] | NS5A2.5 [13] | NS5A5 [12] | NS5A7.5 [12] | NS5A10 [13] | NS5A12.5 [11] |
| | $AgF_2$ | $AgF_2$ | $AgF_2$ | $AgF_2$ | $AgF_2$ | $AgF_2$ |
| $SiO_2$ | 83.84(41) | 76.18(56) | 70.17(79) | 64.45(91) | 59.49(68) | 51.01(69) |
| $Al_2O_3$ | ---- | 4.96(17) | 9.14(20) | 11.95(84) | 15.54(81) | 20.91(48) |
| $Na_2O$ | 16.34(16) | 19.32(28) | 21.51(60) | 23.49(23) | 24.84(72) | 27.65(56) |
| Total | 100.18 | 100.45 | 100.81 | 99.99 | 99.87 | 99.58 |
| Al/(Al + Si) | 0 | 0.07(1) | 0.13(2) | 0.18(2) | 0.24(2) | 0.33(1) |
| NBO/T | 0.38 | 0.39 | 0.38 | 0.40 | 0.38 | 0.38 |
| | KS3A0[d] [12] | KS3A2.5[d] [12] | KS3A5[d] [12] | KS3A7.5[e] [12] | KS3A10[e] [12] | |
| | $PdCl_2$ | $PdCl_2$ | $PdCl_2$ | $PdCl_2$ | $PdCl_2$ | |
| $SiO_2$ | 67.34 | 60.80 | 55.12 | 46.95(36) | 39.80(40) | |
| $Al_2O_3$ | ---- | 3.54 | 7.09 | 12.17(16) | 16.48(11) | |
| $K_2O$ | 33.2 | 35.36 | 37.65 | 41.29(16) | 43.91(13) | |
| Total | 100.56 | 99.7 | 99.86 | 100.41 | 100.19 | |
| Al/(Al + Si) | 0 | 0.06 | 0.13 | 0.23(1) | 0.33(1) | |
| NBO/T | 0.63 | 0.63 | 0.63 | 0.63 | 0.62 | |
| | KS5A0 [12] | KS5A2.5 [12] | KS5A5 [11] | KS5A7.5 [11] | KS5A10 [12] | |
| | $AgF_2$ | $AgF_2$ | $AgF_2$ | $AgF_2$ | $AgF_2$ | |

| | | | | | |
|---|---|---|---|---|---|
| $SiO_2$ | 76.79(60) | 68.94(53) | 61.88(40) | 57.37(41) | 51.22(24) |
| $Al_2O_3$ | ---- | 4.67(5) | 9.00(10) | 11.28(54) | 14.33(9) |
| $K_2O$ | 22.62(20) | 26.29(19) | 29.21(19) | 30.73(52) | 33.71(36) |
| Total | 99.41 | 99.90 | 100.09 | 99.38 | 99.26 |
| Al/(Al + Si) | 0 | 0.07(1) | 0.15(1) | 0.19(1) | 0.25(1) |
| NBO/T | 0.38 | 0.38 | 0.37 | 0.37 | 0.38 |

| | NS4A0 [12] | NS4A5 [12] | NS4A10 [11] |
|---|---|---|---|
| | $AgF_2$ or $PdCl_2$ | $AgF_2$ or $PdCl_2$ | $AgF_2$ or $PdCl_2$ |
| $SiO_2$ | 79.65(55) | 68.16(43) | 54.03(38) |
| $Al_2O_3$ | ---- | 7.96(14) | 17.21(32) |
| $Na_2O$ | 19.74(21) | 24.51(19) | 29.37(29) |
| Total | 99.4 | 100.62 | 100.62 |
| Al/(Al + Si) | 0 | 0.12(1) | 0.27(1) |
| NBO/T | 0.48 | 0.49 | 0.49 |

839
840 Numbers in brackets indicate number of individual electron microscope analyses included on
841 average.
842 Number in parentheses represents one standard deviation in terms of the least units cited.
843 [a] Operating conditions are presented in the text.
844 [b] Calculated from composition assuming that $Si^{4+}$ and $Al^{3+}$ are in tetrahedral coordination in
845 the glasses. Error on Al/(Al + Si) calculated from oxide standard deviations.
846 [c] NBO/T calculated following Mysen and Richet (2005; Chapter 4):
847 $NBO/T = (4 \bullet X_T - 2 \bullet X_O)/X_T$, where $X_T$ and $X_O$ are the atomic proportions of tetrahedrally
848 coordinated cations (Si and Al) and oxygen, respectively.

849 [d] Theoretical composition, calculated from weighing (see text).

850 [e] Composition calculated from extrapolation to 0 seconds of variable counting times during

851 SEM analysis (see text).

852

853

854

855

856

857

858

859

860

861

862

863

864

865

866

867

868

869

870

871 Table 2: Run product compositions in mol% normalized to 100 mol% at 1.5 GPa.

872

## Solubility Samples

| | F10NS5A0 [12] | F10NS5A2.5 [9] | F10NS5A5 [12] | F10NS5A7.5 [11] | F10NS5A10 [14] | F10NS5A12.5 [12] |
|---|---|---|---|---|---|---|
| $SiO_2$ | 76.79(83) | 73.88(61) | 70.33(88) | 64.40(48) | 59.82(37) | 48.28(66) |
| $Al_2O_3$ | | 2.88(12) | 5.21(10) | 7.23(8) | 10.08(11) | 12.18(59) |
| $Na_2O$ | 19.88(23) | 19.20(24) | 20.16(31) | 23.05(30) | 23.79(11) | 32.13(55) |
| F | 3.33(73) | 4.03(79) | 4.29(36) | 5.32(28) | 6.31(37) | 7.40(8) |

| | F10KS5A0 [10] | F10KS5A2.5 [15] | F10KS5A5 [11] | F10KS5A7.5 [13] | F10KS5A10 [11] |
|---|---|---|---|---|---|
| $SiO_2$ | 79.46(61) | 74.57(5) | 69.70(5) | 65.16(54) | 60.81(47) |
| $Al_2O_3$ | | 2.97(9) | 5.95(9) | 7.35(10) | 9.42(9) |
| $K_2O$ | 17.18(8) | 18.03(15) | 19.25(16) | 21.93(18) | 23.23(16) |
| F | 3.36(23) | 4.43(5) | 5.10(57) | 5.56(63) | 6.52(55) |

| | C5NS3A0* [12] | C5NS3A2.5 [15] | C5NS3A5 [10] | C5NS3A7.5 [10] | C5NS3A10 [12] | C5NS3A12.5 [13] |
|---|---|---|---|---|---|---|
| $SiO_2$ | 79.89(243) | 72.53(138) | 68.67(43) | 66.21(42) | 61.48(45) | 53.44(79) |
| $Al_2O_3$ | | 2.69(7) | 5.03(3) | 8.30(5) | 11.10(16) | 14.66(26) |
| $Na_2O$ | 14.41(62) | 19.48(42) | 22.36(26) | 21.99(3) | 24.32(26) | 29.43(53) |
| Cl | 5.70(65) | 4.91(18) | 3.94(66) | 3.49(26) | 3.09(38) | 2.45(30) |

| | C5KS3A0* [11] | C5KS3A2.5* [12] | C5KS3A5* [10] | C5KS3A7.5 [12] | C5KS3A10 [12] |
|---|---|---|---|---|---|
| $SiO_2$ | 85.45(62) | 80.32(66) | 76.58(83) | 69.96(76) | 61.55(62) |
| $Al_2O_3$ | | 2.76(7) | 6.08(10) | 8.85(12) | 10.39(52) |

| | | | | | |
|---|---|---|---|---|---|
| $K_2O$ | 10.92(21) | 14.04(22) | 15.04(30) | 19.41(35) | 26.92(252) |
| Cl | 3.63(21) | 2.87(46) | 2.30(47) | 1.78(35) | 1.14(20) |

Raman Samples

| | F10NS4A0 [12] | F10NS4A5 [12] | F10NS4A10** [12] | C5NS4A0 [12] | C5NS4A5 [12] | C5NS4A10 [11] |
|---|---|---|---|---|---|---|
| $SiO_2$ | 76.78(77) | 66.06(174) | 55.74(146) | 80.42(126) | 74.38(164) | 60.26(105) |
| $Al_2O_3$ | | 5.00(19) | 11.44(33) | | 5.06(20) | 11.50(74) |
| $Na_2O$ | 19.18(42) | 23.88(132) | 25.60(121) | 15.12(87) | 17.17(90) | 25.76(183) |
| F & Cl | 4.42(18) | 5.06(41) | 7.21(58) | 4.46(9) | 3.38(12) | 2.48(13) |

Numbers in brackets indicate number of individual electron microprobe analyses included on average.

Number in parentheses represents one standard deviation in terms of the least units cited.

* $Na_2O$ or $K_2O$ loss during analysis

880

881 Table 3: Run product compositions in mol% normalized to 100 mol% between 1 and 2.5 GPa.

| | F10NS5A0 | | | | F10NS5A5 | | | | F10NS5A10 | | | |
|---|---|---|---|---|---|---|---|---|---|---|---|---|
| GPa | 1 * | 1.5 | 2 | 2.5 | 1 | 1.5 | 2 | 2.5 | 1 | 1.5 | 2 | 2.5 |
| $SiO_2$ | 85.49(94) | 76.79(83) | 80.16(172) | 75.95(84) | 72.71(32) | 70.33(88) | 71.40(38) | 68.17(76) | 57.67(69) | 59.82(37) | 57.25(69) | 58.29(70) |
| $Al_2O_3$ | --- | --- | --- | --- | 5.37(16) | 5.21(10) | 5.38(13) | 5.38(13) | 11.43(42) | 10.08(11) | 11.18(41) | 10.43(38) |
| $Na_2O$ | 11.59(3) | 19.88(23) | 15.66(14) | 19.92(5) | 17.84(9) | 20.16(31) | 17.53(18) | 19.91(28) | 25.24(101) | 23.79(11) | 24.85(99) | 23.71(95) |
| F | 2.91(39) | 3.33(73) | 4.19(66) | 4.56(90) | 4.08(31) | 4.29(36) | 5.69(79) | 6.11(122) | 5.65(17) | 6.31(37) | 6.72(20) | 7.57(23) |
| | F10KS5A0 | | | | F10KS5A5 | | | | F10KS5A10 | | | |
| GPa | 1 | 1.5 | 2* | 2.5 | 1 | 1.5 | 2 | 2.5 | 1 | 1.5 | 2 | 2.5 |
| $SiO_2$ | 80.58(105) | 79.46(61) | 82.50(107) | 81.58(20) | 73.21(36) | 69.70(5) | 68.99(66) | 69.92(41) | 63.51(127) | 60.81(47) | 60.74(99) | 61.28(60) |
| $Al_2O_3$ | --- | --- | --- | --- | 6.13(9) | 5.95(9) | 5.80(17) | 6.02(1) | 11.46(22) | 9.42(9) | 12.57(1) | 10.29(18) |
| $K_2O$ | 16.99(86) | 17.18(8) | 13.92(88) | 14.31(178) | 16.14(271) | 19.25(16) | 19.07(165) | 17.07(124) | 19.13(110) | 23.23(16) | 22.38(262) | 20.63(81) |
| F | 2.43(42) | 3.36(23) | 3.58(61) | 4.10(27) | 4.51(10) | 5.10(57) | 6.14(51) | 6.99(65) | 5.79(29) | 6.52(55) | 7.24(33) | 7.80(36) |
| | C5NS3A0 | | | | C5NS3A5 | | | | C5NS3A10 | | | |
| GPa | 1 | 1.5 | 2 | 2.5 | 1 | 1.5 | 2 | 2.5 | 1 | 1.5 | 2 | 2.5 |
| $SiO_2$ | 78.10(172) | 79.89(243) | 78.55(151) | 79.49(75) | 71.18(58) | 68.67(43) | 70.38(39) | 72.32(34) | 61.39(59) | 61.48(45) | 61.29(88) | 63.04(37) |

| | | | | | | | | | | | | |
|---|---|---|---|---|---|---|---|---|---|---|---|---|
| $Al_2O_3$ | --- | --- | --- | --- | 5.11(18) | 5.03(3) | 5.01(12) | 5.13(11) | 11.05(27) | 11.10(16) | 11.09(38) | 11.20(17) |
| $Na_2O$ | 18.67(39) | 14.41(62) | 14.40(57) | 12.28(25) | 20.18(45) | 22.36(26) | 19.53(43) | 16.66(21) | 24.66(37) | 24.32(26) | 23.66(35) | 21.30(26) |
| Cl | 3.23(11) | 5.70(65) | 7.05(106) | 8.23(103) | 3.42(28) | 3.94(66) | 5.08(34) | 5.89(62) | 2.89(11) | 3.09(38) | 3.94(64) | 4.46(33) |

| | C5KS3A0 | | | | C5KS3A5 | | | | C5KS3A10 | | | |
|---|---|---|---|---|---|---|---|---|---|---|---|---|
| GPa | 1* | 1.5* | 2 | 2.5* | 1 | 1.5 | 2 | 2.5 | 1 | 1.5 | 2 | 2.5 |
| $SiO_2$ | 84.20(74) | 85.45(62) | 81.27(141) | 84.79(49) | 74.42(136) | 76.58(83) | 74.57(108) | 74.58(100) | 61.33(85) | 61.55(62) | 60.56(63) | 60.45(127) |
| $Al_2O_3$ | --- | --- | --- | --- | 5.86(7) | 6.08(10) | 5.98(7) | 6.29(12) | 13.13(23) | 10.39(52) | 11.82(3) | 11.87(13) |
| $K_2O$ | 12.84(10) | 10.92(21) | 14.71(20) | 10.74(5) | 17.63(100 | 15.04(30) | 16.76(16) | 16.16(4) | 24.59(10) | 26.92(252) | 26.45(10) | 26.23(11) |
| Cl | 2.96(23) | 3.63(21) | 4.02(15) | 4.46(33) | 2.09(64) | 2.30(47) | 2.69(1) | 2.97(14) | 0.94(7) | 1.14(20) | 1.17(50) | 1.46(93) |

882 Number in parentheses represents one standard deviation in terms of the least units cited.

883 * $Na_2O$ or $K_2O$ loss during analysis

884 Table 4: Parameters resulting from Raman spectra deconvolutions: Raman shift ($cm^{-1}$), full-
885 width at half maximum height (FWHM, $cm^{-1}$) and intensity.

886

| | NS4 | NS4A5 | NS4A10 | F10NS4 | F10NS4A5 | F10NS4A10 | C5NS4 | C5NS4A5 | C5NS4A10 |
|---|---|---|---|---|---|---|---|---|---|
| Raman Shift | | | | | | | | | |
| 890 band [a] | --- | --- | --- | --- | --- | --- | 905(2) | 894(6) | 882(3) |
| $Q^2$ | 957(0.1) | 966(2) | 945(2) | 957(1) | 964(2) | 973(6) | 990(4) | 962(19) | 949(6) |
| Si-F | --- | --- | --- | 993(0.5) | 1000(2) | 1001(9) | --- | --- | --- |
| Si-Oº | 1046(0.3) | 1049(4) | 1006(3) | 1049(1) | 1052(3) | 1027(7) | 1050(0.6) | 1010(8) | 1005(5) |
| $Q^3$ | 1098(0.5) | 1090(4) | 1051(4) | 1099(1) | 1089(3) | 1064(6) | 1095(0.4) | 1068(2) | 1057(3) |
| $Q^{4\,II}$ | 1148(1) | 1117(6) | 1190(3) | 1145(2) | 1117(3) | 1098(5) | 1146(1) | 1110(1) | 1098(3) |
| $Q^{4\,I}$ | 1181(6) | 1156(8) | 1143(4) | 1183(5) | 1151(5) | 1148(12) | 1171(4) | 1157(6) | 1147(6) |
| $CO_3^{2-}$ [b] | --- | --- | --- | --- | --- | 1065(1) | --- | --- | 1063(0.5) |
| FWHM | | | | | | | | | |
| 890 band [a] | --- | --- | --- | --- | --- | --- | 28(2) | 15(6) | 20(2) |
| $Q^2$ | 29(0.4) | 39(1) | 37(1) | 31(1) | 37(1) | 51(3) | 41(2) | 42(13) | 40(6) |
| Si-F | --- | --- | --- | 15(0.4) | 20(3) | 15(0.1) | --- | --- | --- |
| Si-Oº | 35(1) | 36(0.1) | 33(3) | 37(2) | 35(4) | 32(3) | 31(3) | 34(9) | 44(4) |
| $Q^3$ | 31(0.5) | 30(0.1) | 30(0.1) | 30(0.5) | 30(0.1) | 30(0.1) | 30(1) | 32(0.1) | 32(0.1) |
| $Q^{4\,II}$ | 25(2) | 34(4) | 35(2) | 26(2) | 29(1) | 37(3) | 23(1) | 32(2) | 34(2) |
| $Q^{4\,I}$ | 32(2) | 37(4) | 44(1) | 27(3) | 34(2) | 43(2) | 38(2) | 41(2) | 40(2) |
| $CO_3^{2-}$ [b] | --- | --- | --- | --- | --- | --- | --- | --- | 9(0.3) |
| Intensity | | | | | | | | | |

| | | | | | | | | | |
|---|---|---|---|---|---|---|---|---|---|
| 890 band [a] | --- | --- | --- | --- | --- | --- | 2(0.1) | 2(1) | 3(1) |
| $Q^2$ | 5(0.1) | 14(0.3) | 32(2) | 13(0.1) | 15(0.5) | 19(2) | 10(1) | 13(6) | 14(4) |
| Si-F | --- | --- | --- | 10(1) | 7(2) | 2(1) | --- | --- | --- |
| Si-Oº | 20(0.5) | 34(4) | 48(4) | 37(1) | 41(3) | 16(3) | 23(1) | 22(5) | 37(3) |
| $Q^3$ | 93(1) | 51(11) | 48(5) | 85(3) | 58(8) | 32(4) | 91(1) | 73(6) | 49(4) |
| $Q^{4\,II}$ | 29(5) | 48(8) | 73(6) | 31(2) | 38(5) | 31(3) | 19(3) | 54(3) | 61(5) |
| $Q^{4\,I}$ | 18(3) | 15(5) | 13(2) | 13(2) | 22(4) | 5(4) | 22(2) | 30(2) | 23(3) |
| $CO_3^{2-}$ [b] | --- | --- | --- | --- | --- | --- | --- | --- | 10(1) |

887

888 Number in parentheses represents one standard deviation in terms of the least units cited.

889 [a] see assignment discussion in the text.

890 [b] contamination, see Fig. 5.

891

892 Table 5: Comparison of $\chi^2$ from fits to F-bearing NS4Ax melts.

| | $\chi^2$ w/ 990 $cm^{-1}$ band | $\chi^2$ w/o 990 $cm^{-1}$ band |
|---|---|---|
| F10NS4 | 2.6 | 15.8 |
| F10NS4A5 | 22.0 | 18.6 |
| F10NS4A10 | 5.4 | 10.5 |

893
894
895
896
897
898
899
900
901
902
903
904
905
906
907
908
909
910
911

Table 6: Species abundance from Raman spectra of melts.

| | Relative peak area | | | Δ NBO/T |
|---|---|---|---|---|
| | $Q^2$ | $Q^3$ | $Q^{4\,a}$ | |
| NS4 | 0.04(0.2) | 0.67(4) | 0.30(11) | --- |
| NS4A5 | 0.12(2) | 0.36(9) | 0.52(28) | --- |
| NS4A10 | 0.20(2) | 0.25(3) | 0.55(9) | --- |
| F10NS4 | 0.10(1) | 0.62(10) | 0.29(9) | 0.33(10) |
| F10NS4A5 | 0.13(2) | 0.42(9) | 0.44(14) | 0.20(9) |
| F10NS4A10 | 0.29(5) | 0.29(6) | 0.42(35) | 0.23(8) |
| C5NS4 | 0.09(1) | 0.62(12) | 0.28(4) | 0.33(12) |
| C5NS4A5 | 0.09(7) | 0.40(9) | 0.51(16) | 0.10(9) |
| C5NS4A10 | 0.11(4) | 0.30(5) | 0.59(9) | 0.03(7) |

Errors on $Q^n$ species abundances were recalculated following the method of Mysen (2007). To calculate the $Q^n$-species mole fractions, the area of bands around 990, 1010–1050, and 1065 $cm^{-1}$ were not taken into account.

[a] Sum of $Q^{4,I}$ and $Q^{4,II}$

936 FIGURES

937

938 Figure 1

939

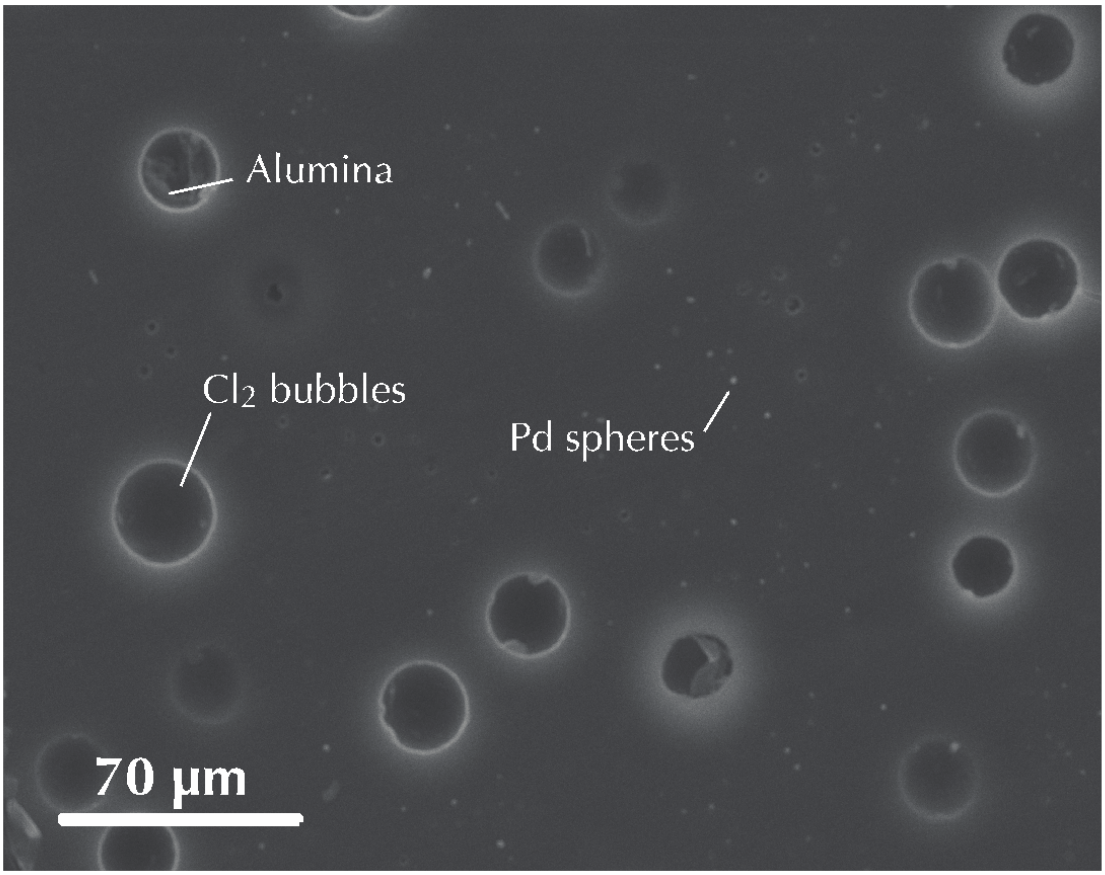


940

941

942

943

944

945

946

947

948 Figure 2

949

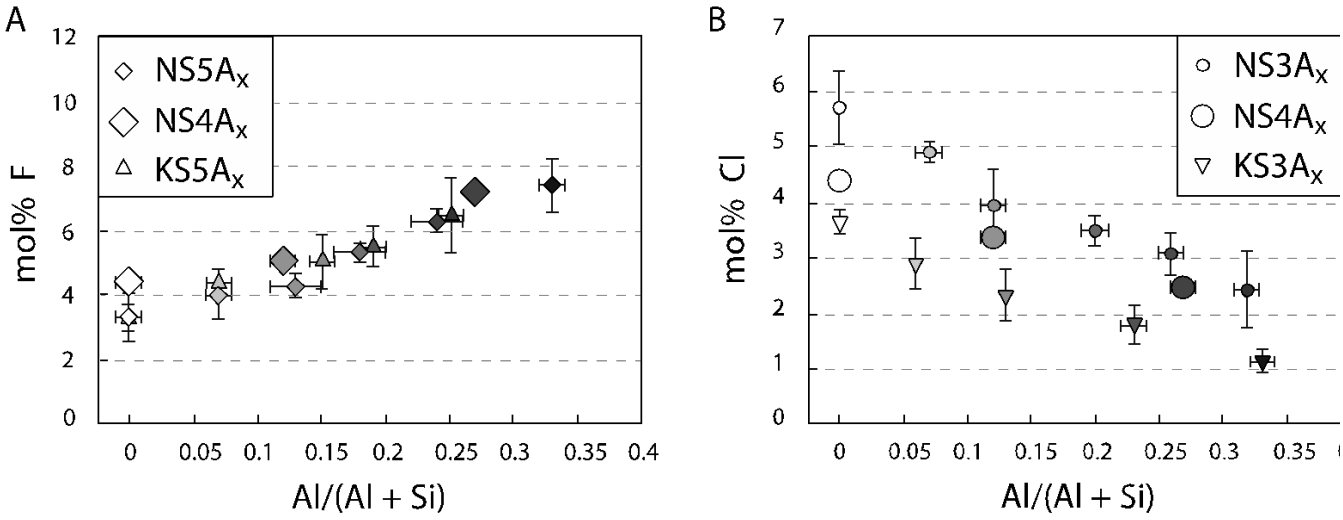


950

951

952

953

954

955

956

957

958

959

960

961

962

963

964

965 Figure 3

966

967

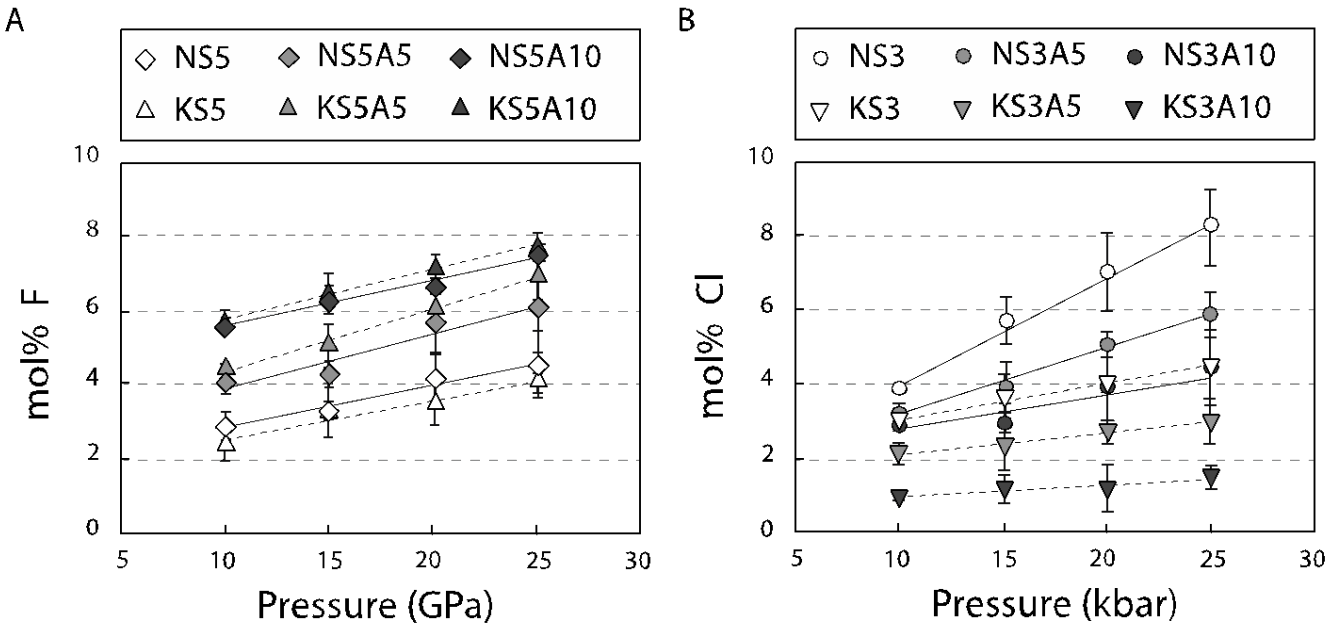


968

969

970

971

972

973

974

975

976

977

978

979

980 Figure 4

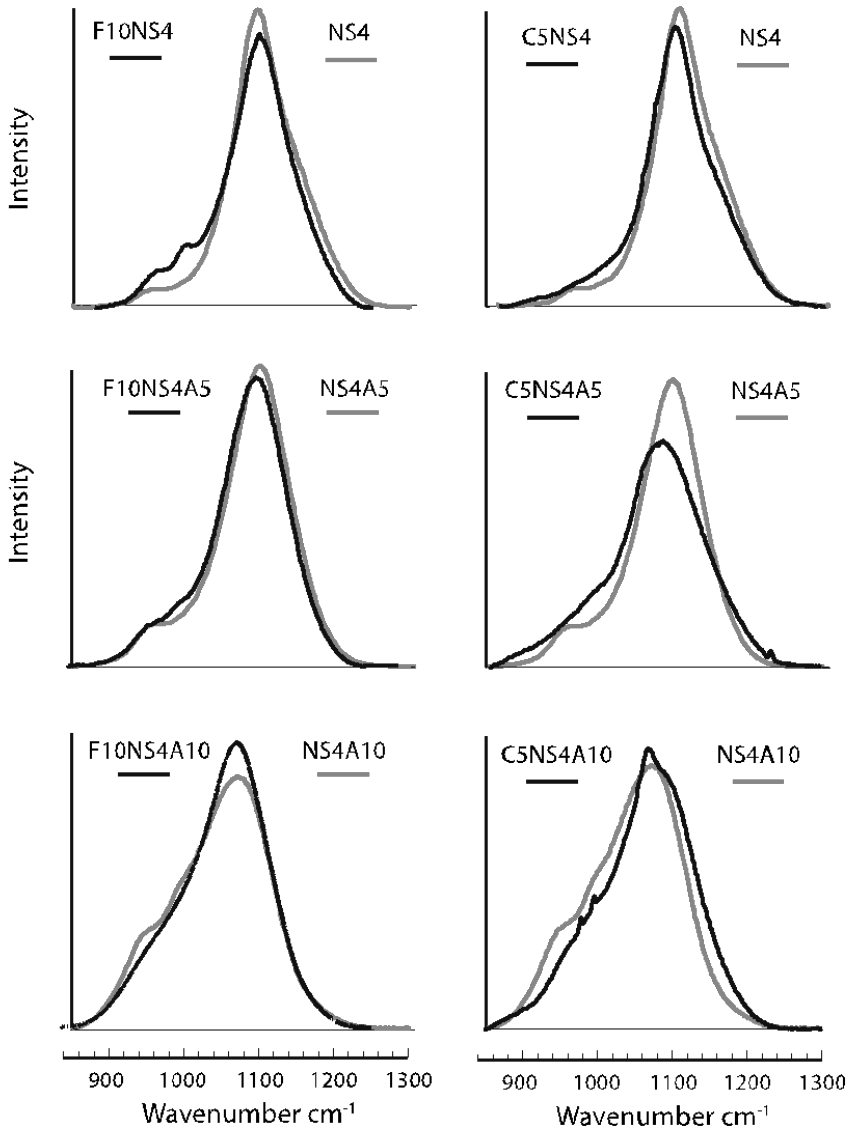


981

982

983

984

985

986

987

988 Figure 5

989

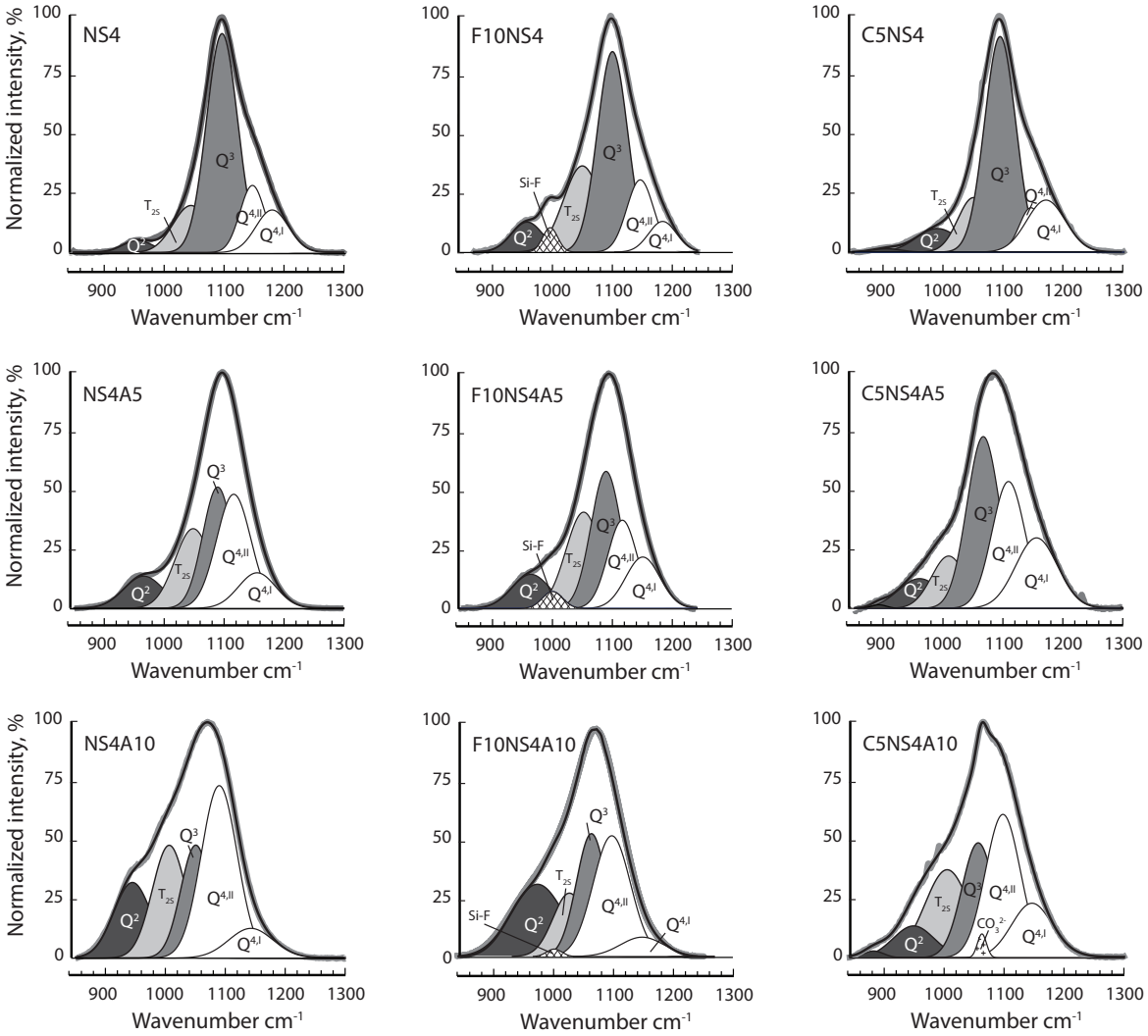


990

991

992

993

994

995

996

997

998 Figure 6

999

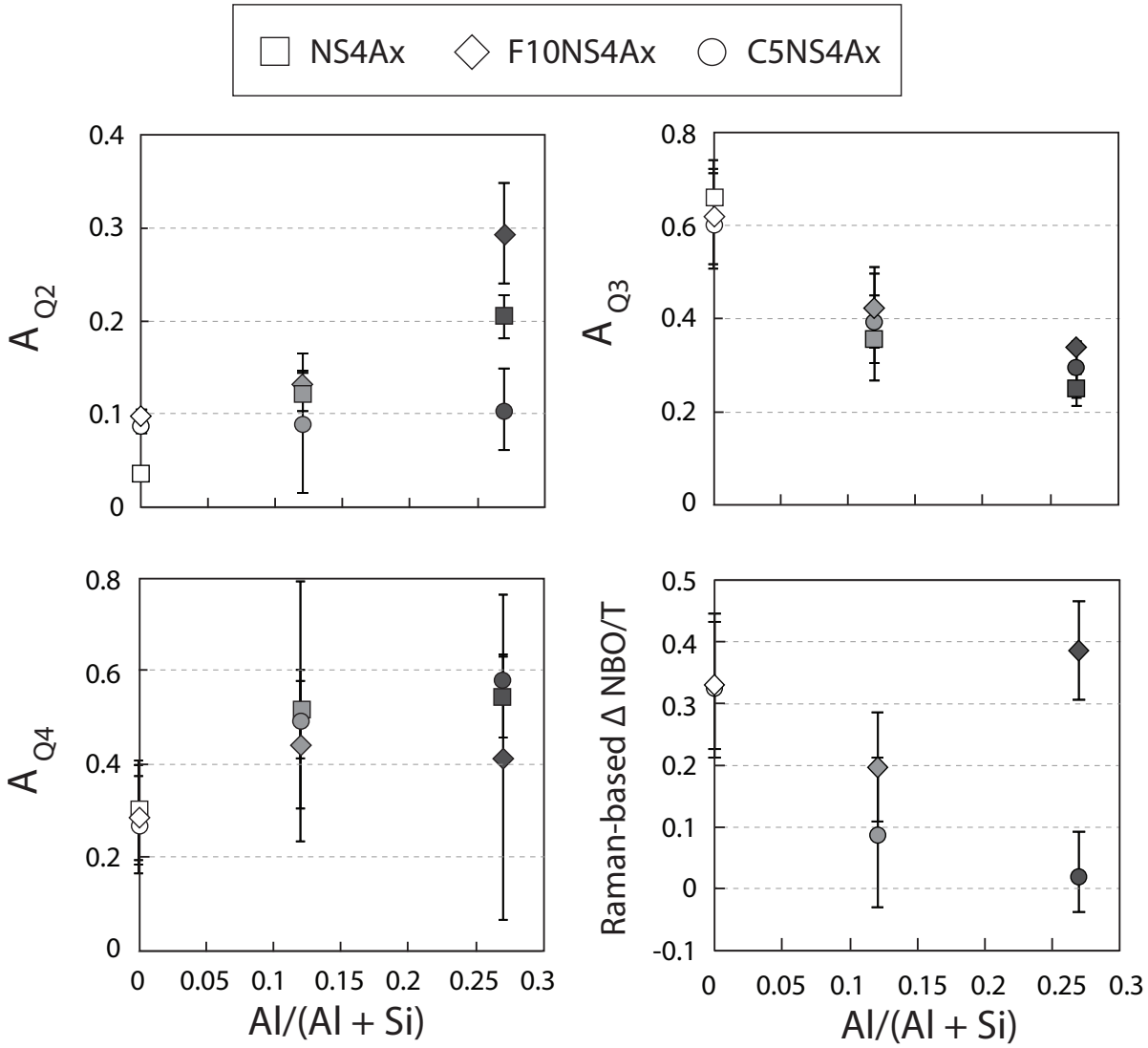


1000